

Study of Three Generation Seesaw Model with
Dirac Mass Matrix of Four-zero Texture and CP
Violation in Neutrino Sector

Akihiro Yuu

Department of Physical Science
Graduate School of Science
Hiroshima University

2020

Abstract

We introduce the four-zero texture models on the neutrino Dirac mass matrix and suggest a classification for those textures to investigate the number of non-zero neutrino mass eigenvalues and the presence of CP violation in the neutrino sector. Four-zero texture model on the Dirac mass matrix includes seven model parameters in the context of type-I seesaw mechanism. This number of model parameters is less than that of the general description of the Majorana mass matrix with three right-handed Majorana neutrinos; three neutrino mass eigenvalues, three mixing angles and three CP violating phases. The efficient method is proposed to perform the numerical analysis for four-zero texture models. We show some results of the numerical calculations as for correlations among model parameters, neutrino mass eigenvalues and CP violating phases. These correlations can be explained by the relations arising from the elements of the effective Majorana mass matrix with four-zero texture. The position of a non-zero element on the effective Majorana mass matrix, which is associated with the classification for four-zero textures, fixes the constraints among parameters. The Majorana mass matrix all of whose elements are non-vanishing also produce other relations particularly in the case of four-zero textures.

Title of Doctoral Thesis

- Study of three generation seesaw model with Dirac mass matrix of four-zero texture and CP violation in neutrino sector

Title of the published article on which the thesis is mainly based

- Takuya Morozumi, Yusuke Shimizu, Hiroyuki Umeeda and Akihiro Yuu, Hidden relations in three generation seesaw model with Dirac mass matrix of four-zero texture, *Phys.Lett.* B799 (2019) 135046.

Contents

1	Introduction	4
2	Physics in the neutrino sector	5
2.1	Seesaw mechanism	5
2.2	Mixing and CP phases	6
2.3	CP asymmetry in the neutrino sector	6
3	Model	8
3.1	Model and parameters	8
3.2	Four-zero texture model on Dirac mass matrix	8
3.3	Seesaw model with one massless neutrino	9
4	Classification of four-zero textures	11
5	Numerical analysis	13
5.1	How to perform the numerical analysis	13
5.2	Sub-classification	15
5.3	Results	17
5.3.1	Correlations among model parameters	18
5.3.2	Correlations among mass eigenvalues	18
5.3.3	Correlations among CP phases	25
6	Analyses with hidden relations among elements of Majorana mass matrix	25
6.1	Constraints from vanishing elements on m_{eff}	25
6.2	Explanations for the results of numerical analysis	35
6.2.1	$(m_{\text{eff}})_{e\mu} = 0$ in IH case	35
6.2.2	$(m_{\text{eff}})_{e\tau} = 0$ in IH case	35
6.2.3	$(m_{\text{eff}})_{\mu\tau} = 0$ in NH case	37
6.2.4	subclass (II)-B in IH case	37
6.2.5	$(m_{\text{eff}})_{e\tau} = 0$ in NH case	37
7	Discussions and Summary	39
8	Appendix	40
8.1	The general Δ with full elements of the Dirac mass matrix	40
8.2	The m_{eff} and Δ with concrete parametrization for each class	42

1 Introduction

Neutrino is a kind of lepton, which does not have electric charge. It is known that neutrino has tiny but non-zero mass by the neutrino oscillation. However, Standard Model(SM) can not explain their mass, since it includes only left-handed neutrinos and can not construct their mass terms. Seesaw mechanism has been suggested to describe their masses and to understand why they are so tiny [12]. It extends SM by introducing heavy right-handed neutrinos and by assuming that they are Majorana particles. We study the type-I seesaw model with three right-handed neutrinos. This mechanism leads to effective Majorana mass term for light active neutrinos. It is written with Dirac mass matrix and Majorana mass matrix for right-handed neutrinos.

the Dirac mass matrix and the Majorana mass matrix are parametrized by 15 and 3 parameters respectively in the real diagonal basis for the Majorana mass matrix and charged-lepton mass matrix. The effective mass matrix is then expressed by 18 parameters. The general model still has much parameters by comparing with the number of phenomenological parameters; three mass eigenvalues, three mixing angles and three CP phases. In this paper, we focus on the four-zero texture model for the Dirac mass matrix [16, 13, 14, 17]. We put four zero-elements onto the Dirac mass matrix by hand. The other five elements remain non-zero. The effective mass matrix of four-zero texture model is parametrized with seven parameters, which are comparable to the number of measurements.

There are ${}_9C_4 = 126$ different configurations of Dirac mass matrix of four-zero texture model. We develop an efficient method to explore all the configurations without examining each form independently. In the method, different form of Dirac matrices related to each other by permutation of their rows and columns are classified into several groups. Phenomenological constraints on the parameters are also imposed according to this classification.

Some flavor symmetries restrict the forms of the Dirac mass matrix and the Majorana mass matrix [13, 14, 15]. Flavor symmetry reduces the number of model parameters. The position of zeros on the Dirac mass matrix can be restricted by some flavor symmetries.

The paper is organized as follows. In section 2, we introduce the type-I seesaw mechanism which explains the tiny but non-zero masses of neutrino. We also mention the CP asymmetry in the neutrino sector via neutrino oscillation. In section 3, we define the notation of our model by using the type-I seesaw mechanism with three heavy right-handed Majorana neutrinos. We suggest two specific models; four-zero texture model on Dirac mass matrix in subsection 3.2 and seesaw model with one massless neutrino in subsection 3.3. In section 4, we study the four-zero texture model on Dirac mass matrix. The 126 different patterns of zero-elements-configuration on the Dirac mass matrix are classified into 7 classes. This classification serves for sorting which textures we have to analyze. In section 5, we make numerical analysis. We first outline how to perform the numerical analysis and then explain the efficient method according to the classification of textures. Some results of calculations are shown in subsection 5.3. In section 6, the hidden relations among the elements of the effective Majorana mass are derived and the correlations found in the numerical analysis are examined from a view point of the hidden relations. Section 7 is devoted to the summary.

2 Physics in the neutrino sector

2.1 Seesaw mechanism

Standard Model (SM) does not include any mass terms for neutrino. It needs to modify the theory according to the existence of neutrino masses. The seesaw mechanism is suggested as an attractive extension of SM to explain the neutrino masses and also to understand why are they so tiny.

Since neutrino has no electric charge, it is possible that a neutrino and its antiparticle are identical to each other. Such a fermion is called as Majorana fermion. It has yet to be confirmed if neutrino is Majorana or not. Neutrino-less double beta decay, for example, is expected to be an evidence of that. To construct the seesaw mechanism, we assume that neutrino is a Majorana particle and introduce heavy right-handed neutrinos, which are absent in SM.

The most general neutrino mass term is

$$\mathcal{L}_m = -\frac{1}{2}m_L(\bar{\nu}_L)^c\nu_L - \frac{1}{2}m_R(\bar{\nu}_R)^c\nu_R - m_D\bar{\nu}_L\nu_R + h.c., \quad (1)$$

where m_L and m_R are the Majorana masses of left- and right-handed neutrinos respectively, m_D is Dirac mass. Eq.(1) can be rewritten to

$$\mathcal{L}_m = -\frac{1}{2}(\bar{\nu})^c m_\nu \nu + h.c., \quad (2)$$

where

$$\nu \equiv \begin{pmatrix} \nu_L \\ (\nu_R)^c \end{pmatrix} \quad (3)$$

and

$$m_\nu \equiv \begin{pmatrix} m_L & m_D \\ m_D^\dagger & m_R^* \end{pmatrix}. \quad (4)$$

m_ν is a 6 by 6 complex symmetric matrix. Let us take $m_L = 0$ and use a real-diagonalized right-handed Majorana mass matrix

$$m_R = M = \text{diag}(M_1, M_2, M_3). \quad (5)$$

$$m_\nu = \begin{pmatrix} 0 & m_D \\ m_D^\dagger & M \end{pmatrix}. \quad (6)$$

Eq.(6) is block-diagonalized by an Unitary matrix

$$U = \begin{pmatrix} iI & m_D^\dagger M^{-1} \\ -iM^{-1}m_D & I \end{pmatrix}. \quad (7)$$

I is the 3 by 3 unit matrix $I = \text{diag}(1, 1, 1)$.

$$Um_\nu U^t \simeq \begin{pmatrix} -m_{eff} & 0 \\ 0 & M \end{pmatrix}. \quad (8)$$

The basis is converted as

$$\nu' \equiv U^* \nu = \begin{pmatrix} -i\nu_L \\ (\nu_R)^c \end{pmatrix} \quad (9)$$

We define the effective matrix as

$$m_{eff} \equiv -m_D M^{-1} m_D^t. \quad (10)$$

$$\begin{aligned} \mathcal{L}_m &= -\frac{1}{2}((\overline{\nu_L})^c, \overline{\nu_R}) \begin{pmatrix} 0 & m_D \\ m_D^t & M \end{pmatrix} \begin{pmatrix} \nu_L \\ (\nu_R)^c \end{pmatrix} + h.c. \\ &\simeq -\frac{1}{2}((\overline{\nu'_L})^c, \overline{\nu'_R}) \begin{pmatrix} -m_{eff} & 0 \\ 0 & M \end{pmatrix} \begin{pmatrix} \nu'_L \\ (\nu'_R)^c \end{pmatrix} + h.c. \\ &= \frac{1}{2}(\overline{\nu'_L})^c m_{eff} \nu'_L + \frac{1}{2}\overline{\nu'_R} M (\nu'_R)^c + h.c. \end{aligned} \quad (11)$$

The first term on the last line of Eq.(11) correspond to the mass term of the active neutrino. The second term is interpreted as the mass term of the sterile neutrino which hardly interacts with other particles. Since its mass is much larger than the weak scale, it is decoupled from the experimentally achievable energy theory. We can thus detect only the active neutrino with tiny mass.

2.2 Mixing and CP phases

The effective mass matrix Eq.(10) is real-diagonalized by an Unitary matrix and produces three neutrino mass eigenvalues under the condition that charged leptons are in the diagonal basis.

$$V_{PMNS}^\dagger m_{eff} (V_{PMNS})^* = \begin{pmatrix} m_1 & 0 & 0 \\ 0 & m_2 & 0 \\ 0 & 0 & m_3 \end{pmatrix}. \quad (12)$$

m_i ($i = 1, 2, 3$) are the neutrino mass eigenvalues. The Unitary matrix V_{PMNS} which real-diagonalizes m_{eff} is called as Pontecorvo-Maki-Nakagawa-Sakata matrix (PMNS matrix). A conventional parametrization for PMNS matrix is

$$V_{PMNS} = \begin{pmatrix} c_{12}c_{13} & s_{12}c_{13} & s_{13}e^{-i\delta} \\ -s_{12}c_{23} - c_{12}s_{23}s_{13}e^{i\delta} & c_{12}c_{13} - s_{12}s_{23}s_{13}e^{i\delta} & s_{23}c_{13} \\ s_{12}s_{23} - c_{12}c_{23}s_{13}e^{i\delta} & -c_{12}s_{23} - s_{12}c_{23}s_{13}e^{i\delta} & c_{23}c_{13} \end{pmatrix} \begin{pmatrix} 1 & 0 & 0 \\ 0 & e^{i\frac{\alpha_{21}}{2}} & 0 \\ 0 & 0 & e^{i\frac{\alpha_{31}}{2}} \end{pmatrix}, \quad (13)$$

where $s_{ij} = \sin \theta_{ij}$, $c_{ij} = \cos \theta_{ij}$. θ_{12} , θ_{23} and θ_{31} are the neutrino mixing angles. δ is a non-vanishing Dirac CP phase. If neutrino is a Majorana fermion, V_{PMNS} includes extra two Majorana CP phases α_{21} , α_{31} .

The flavor-basis and the mass-basis of neutrino is related to each other by means of V_{PMNS} .

$$V_{PMNS} \begin{pmatrix} \nu_1 \\ \nu_2 \\ \nu_3 \end{pmatrix} = \begin{pmatrix} \nu_e \\ \nu_\mu \\ \nu_\tau \end{pmatrix}. \quad (14)$$

2.3 CP asymmetry in the neutrino sector

Neutrino oscillation is a phenomenon by which a neutrino with specific flavor changes to that with another flavor during the propagation. The probability of measuring a particular flavor of a neutrino is expressed as a function of the distance or of the time how long does it propagate.

The probability that a neutrino generated with the flavor α at $t = 0$ is detected later with the flavor β at t is

$$P(\nu_\alpha \longrightarrow \nu_\beta) = \left| \sum_j (V_{PMNS})_{\beta j} \exp\left\{-i \frac{\Delta m_{ji}^2}{2E} t\right\} (V_{PMNS})_{\alpha j}^* \right|^2. \quad (15)$$

Δm_{ij}^2 are the neutrino mass squared differences

$$\Delta m_{ij}^2 \equiv m_i^2 - m_j^2, \quad (16)$$

where $\alpha, \beta = e, \mu, \tau$ and $i, j = 1, 2, 3$.

We define the CP asymmetry of neutrino oscillation from the flavor α to β as the subtraction of transition probabilities between neutrino and anti-neutrino

$$A_{\alpha\beta}^{CP} \equiv P(\nu_\alpha \longrightarrow \nu_\beta) - P(\bar{\nu}_\alpha \longrightarrow \bar{\nu}_\beta). \quad (17)$$

By calculating Eq.(17),

$$A_{\alpha\beta}^{CP} = -4 \sum_{i < j} J_{\alpha\beta;ij} \sin\left(\frac{\Delta m_{ij}^2}{2E} t\right). \quad (18)$$

where

$$J_{\alpha\beta;ij} \equiv \text{Im}\{U_{\alpha i} U_{\beta i}^* U_{\beta j} U_{\alpha j}^*\}. \quad (19)$$

The following relational expressions about $J_{\alpha\beta;ij}$ hold because of the unitarity of V_{PMNS} .

$$J_{e\mu;ij} = J_{\mu\tau;ij} = J_{\tau e;ij}, \quad (20)$$

$$J_{\alpha\beta;12} = J_{\alpha\beta;23} = J_{\alpha\beta;31}, \quad (21)$$

$$J_{\alpha\beta;ij} = -J_{\beta\alpha;ij}, \quad (22)$$

$$J_{\alpha\beta;ij} = -J_{\alpha\beta;ji}. \quad (23)$$

By defining the Jarlskog invariant [23] as

$$J \equiv J_{e\mu;12}, \quad (24)$$

we obtain the CP asymmetry independent of specific flavors,

$$A^{CP} \equiv A_{e\mu}^{CP} = 16J \sin\left(\frac{\Delta n_{12}^2}{2E} t\right) \sin\left(\frac{\Delta n_{23}^2}{2E} t\right) \sin\left(\frac{\Delta n_{31}^2}{2E} t\right). \quad (25)$$

Inserting the elements of V_{PMNS} described in Eq.(13) into Eq.(24), J is expressed in terms of three mixing angles and the Dirac CP phase,

$$J = s_{12} s_{23} s_{13} c_{12} c_{23} c_{13}^2 \sin \delta. \quad (26)$$

Eq.(25) and Eq.(26) imply that, if any two mass eigenvalues are degenerate and/or if at least one of mixing angles or Dirac CP phase equals to zero, CP symmetry breaking in neutrino sector does not occur.

The Jarlskog invariant can also be expressed in terms of the effective mass matrix and neutrino mass squared differences,

$$J = \frac{\text{Im}((m_{\text{eff}} m_{\text{eff}}^\dagger)_{e\mu} (m_{\text{eff}} m_{\text{eff}}^\dagger)_{\mu\tau} (m_{\text{eff}} m_{\text{eff}}^\dagger)_{\tau e})}{\Delta m_{12}^2 \Delta m_{23}^2 \Delta m_{31}^2}. \quad (27)$$

We define a quantity Δ as the product of Jarlskog invariant and neutrino mass squared differences, i.e. it is the numerator of Eq.(27).

$$\begin{aligned} \Delta &\equiv \text{Im}((m_{\text{eff}} m_{\text{eff}}^\dagger)_{e\mu} (m_{\text{eff}} m_{\text{eff}}^\dagger)_{\mu\tau} (m_{\text{eff}} m_{\text{eff}}^\dagger)_{\tau e}) \\ &= J \Delta m_{12}^2 \Delta m_{23}^2 \Delta m_{31}^2 \end{aligned} \quad (28)$$

3 Model

3.1 Model and parameters

The effective Majorana mass matrix m_{eff} of the seesaw model with three right-handed Majorana neutrino was introduced in Eq.10 in terms of the real diagonal right-handed Majorana mass matrix M and the Dirac mass matrix m_D . We shall use the diagonal basis in charged lepton sector. We name m_{Di} ($i = 1, 2, 3$) as the magnitudes of column vectors of m_D

$$m_D = \mathcal{U} \begin{pmatrix} m_{D1} & 0 & 0 \\ 0 & m_{D2} & 0 \\ 0 & 0 & m_{D3} \end{pmatrix}, \quad \mathcal{U} = \begin{pmatrix} \mathcal{U}_{e1} & \mathcal{U}_{e2} & \mathcal{U}_{e3} \\ \mathcal{U}_{\mu1} & \mathcal{U}_{\mu2} & \mathcal{U}_{\mu3} \\ \mathcal{U}_{\tau1} & \mathcal{U}_{\tau2} & \mathcal{U}_{\tau3} \end{pmatrix}. \quad (29)$$

\mathcal{U} is a non-unitary matrix, which satisfies the following condition

$$\sum_{\alpha=e,\mu,\tau} |\mathcal{U}_{\alpha i}|^2 = 1. \quad (30)$$

The column vectors of \mathcal{U} are normalized. Three of the 9 phases of \mathcal{U} can be rotated away by flavor-basis transformation. The most general \mathcal{U} involves 6 independent moduli and 6 phases. We define a diagonal matrix X as follows

$$X = \begin{pmatrix} X_1 & 0 & 0 \\ 0 & X_2 & 0 \\ 0 & 0 & X_3 \end{pmatrix}, \quad X_i = \frac{m_{Di}^2}{M_i}. \quad (31)$$

Rewriting the m_{eff} in terms of \mathcal{U} and X [22],

$$m_{\text{eff}} = -\mathcal{U}X\mathcal{U}^t. \quad (32)$$

We define A_{ij} as a inner products of \mathbf{u}_i .

$$A_{ij} \equiv \mathbf{u}_i^\dagger \cdot \mathbf{u}_j, \quad (33)$$

and an Hermite matrix A whose elements are A_{ij} ,

$$A \equiv \mathcal{U}^\dagger \mathcal{U} = \begin{pmatrix} 1 & A_{12} & A_{13} \\ A_{21} & 1 & A_{23} \\ A_{31} & A_{32} & 1 \end{pmatrix}. \quad (34)$$

3.2 Four-zero texture model on Dirac mass matrix

A three by three complex matrix \mathcal{U} whose column components are normalized has 15 parameters. There is three degrees of freedom to redefine the phases form charged leptons. By multiplying a appropriate diagonal matrix $diag = (e^\alpha, e^\beta, e^\gamma)$, the number of parameters on \mathcal{U} is reduced to 12. The matrix X consists of three parameters. The general m_{eff} with three right-handed neutrinos is therefore parametrized with 15 independent parameters. It still has many in comparison to 7 experimental observables which include 3 mixing angles, a Dirac CP violating phase, two mass squared differences, and $|(m_{\text{eff}})_{ee}|$.

To reduce the number of model parameters, we substitute 0s in the elements of Dirac mass matrix \mathcal{U} by hand. We set four of nine elements on Dirac mass

matrix 0 and the other five non-zero. The configuration of the four-zero texture in three by three matrix has ${}_9C_4 = 126$ different patterns. We classify all of them into some classes in section 4. We develop then an efficient method to explore all the configurations without examining each form independently in section 5.

Taking into account of the condition that the column vectors of \mathcal{U} are normalized as Eq.(30), 90 out of 126 four-zero textures on \mathcal{U} can be expressed by four parameters after the suitable flavor-basis transformation. For example, one of the four-zero textures is written as

$$\mathcal{U} = \begin{pmatrix} \cos \theta_1 e^{i\phi_1} & \cos \theta_2 e^{i\phi_2} & 1 \\ \sin \theta_1 & 0 & 0 \\ 0 & \sin \theta_2 & 0 \end{pmatrix}, \quad (35)$$

with two angles θ_1, θ_2 and two non-vanishing phases ϕ_1, ϕ_2 . The m_{eff} has seven parameters. Textures in which \mathcal{U} has more than five 0 elements either do not explain the CP asymmetry in neutrino oscillation or result in the minimal seesaw model with two right handed neutrinos, which causes a zero neutrino mass. The four-zeros in \mathcal{U} is the most minimal texture to produce both the CP asymmetry and three non-zero mass eigenvalues of neutrino.

36 textures on \mathcal{U} are expressed with five parameters. 18 textures include three angles $\theta_1, \theta_2, \theta_3$ and two phases ϕ_1, ϕ_2 . An example is as follows.

$$\mathcal{U} = \begin{pmatrix} \sin \theta_1 \cos \theta_2 & \cos \theta_3 e^{i\phi_1} & 0 \\ \sin \theta_1 \sin \theta_2 & \sin \theta_3 e^{i\phi_2} & 0 \\ \cos \theta_1 & 0 & 0 \end{pmatrix}, \quad (36)$$

The other 18 textures on \mathcal{U} are include two angles θ_1, θ_2 and three phases ϕ_1, ϕ_2, ϕ_3 . An example is as follows.

$$\mathcal{U} = \begin{pmatrix} \cos \theta_1 & \cos \theta_2 e^{i\phi_1} & e^{i\phi_3} \\ \sin \theta_1 & \sin \theta_2 e^{i\phi_2} & 0 \\ 0 & 0 & 0 \end{pmatrix}, \quad (37)$$

3.3 Seesaw model with one massless neutrino

One massless neutrino is still allowed consistent with experimental results. In such case the analytical discussion can be easily to handle. The minimal model with two heavy right-handed neutrinos produces automatically one massless neutrino. We discuss the analysis by means of more general model with three right-handed neutrinos.

$$\det \mathcal{U} = 0 \quad (38)$$

is a necessary and sufficient condition for the existence of at least one 0 neutrino mass eigenvalue. Three column components of a three by three matrix whose determinant equals 0 are not independent each other. One of them is described as the linear combination of the others. Let us suppose that \mathcal{U} is a matrix whose rank is 2 to explain two non-zero mass eigenvalues and three mixing angles.

$$\mathcal{U} = (\mathbf{u}_1, \mathbf{u}_2, a\mathbf{u}_1 + b\mathbf{u}_2), \quad (39)$$

where a and b are complex coefficients expressed in terms of the elements of \mathcal{U} .

$$\begin{aligned} a &= \frac{A_{13} - A_{12}A_{23}}{1 - |A_{12}|^2} \\ b &= \frac{A_{23} - A_{21}A_{13}}{1 - |A_{12}|^2} \end{aligned} \quad (40)$$

Since \mathbf{u}_1 and \mathbf{u}_2 are linearly independent, $|\mathbf{u}_1^\dagger \cdot \mathbf{u}_2| < 1$ and $1 - |A_{12}|^2 \neq 0$ is certified. \mathcal{U} with rank 2 can be transformed to a triangular matrix T by an Unitary matrix V using the Gram-Schmidt orthogonal normalization,

$$V^\dagger U = \begin{pmatrix} 0 & 0 & 0 \\ 0 & t_{22} & t_{23} \\ t_{31} & t_{32} & t_{33} \end{pmatrix}. \quad (41)$$

Expressing V and T in terms of the elements of \mathcal{U} ,

$$V \equiv (\mathbf{v}_1, \mathbf{v}_2, \mathbf{v}_3) = \left(\frac{\mathbf{u}_2^* \times \mathbf{u}_1^*}{1 - |A_{12}|^2}, \frac{\mathbf{u}_2 - A_{12}\mathbf{u}_1}{1 - |A_{12}|^2}, \mathbf{u}_1 \right), \quad (42)$$

$$T \equiv \begin{pmatrix} 0 & 0 & 0 \\ 0 & t_{22} & t_{23} \\ t_{31} & t_{32} & t_{33} \end{pmatrix} = \begin{pmatrix} 0 & 0 & 0 \\ 0 & \sqrt{1 - |A_{12}|^2} & \frac{A_{23} - A_{21}A_{13}}{1 - |A_{12}|^2} \\ 1 & A_{21} & A_{13} \end{pmatrix}. \quad (43)$$

t_{31} and t_{21} can be taken real, while t_{23} , t_{32} and t_{33} remain complex. By multiplying T and its transposed matrix by the diagonal matrix X , it is reduced to two by two complex symmetric matrix,

$$TXT^t = - \begin{pmatrix} 0 & 0 & 0 \\ 0 & Z_{22} & Z_{23} \\ 0 & Z_{32} & Z_{33} \end{pmatrix} \equiv -Z, \quad (44)$$

where

$$\begin{aligned} Z_{22} &\equiv X_2(1 - |A_{12}|^2) + X_3(1 - |A_{13}|^2)e^{2i\rho}, \\ Z_{33} &\equiv X_1 + X_2A_{12}^2 + X_3A_{13}^2, \\ Z_{23} &\equiv X_2A_{12}\sqrt{1 - |A_{12}|^2} + X_3A_{13}\sqrt{1 - |A_{13}|^2}e^{i\rho}, \end{aligned} \quad (45)$$

and

$$\rho \equiv \arg(A_{23} - A_{21}A_{13}). \quad (46)$$

Z is real-diagonalized by the matrix K with three parameters χ , σ_1 and σ_2 ,

$$K^\dagger ZK^* = \begin{pmatrix} 1 & 0 & 0 \\ 0 & m_2 & 0 \\ 0 & 0 & m_3 \end{pmatrix}, \quad (47)$$

where

$$\begin{aligned} K &\equiv \begin{pmatrix} 1 & 0 & 0 \\ 0 & \cos \chi & \sin \chi e^{-i\sigma_1} \\ 0 & -\sin \chi e^{i\sigma_1} & \cos \chi \end{pmatrix} \begin{pmatrix} 1 & 0 & 0 \\ 0 & e^{i\sigma_2} & 0 \\ 0 & 0 & e^{-i\sigma_2} \end{pmatrix} \\ &= \begin{pmatrix} 1 & 0 & 0 \\ 0 & \cos \chi e^{i\sigma_2} & \sin \chi e^{-i(\sigma_1 + \sigma_2)} \\ 0 & -\sin \chi e^{i(\sigma_1 + \sigma_2)} & \cos \chi e^{-i\sigma_2} \end{pmatrix}, \end{aligned} \quad (48)$$

and

$$\begin{aligned}
\chi &\equiv \frac{1}{2} \tan^{-1} \left(\frac{2|Z_{22}^* Z_{23} + Z_{23}^* Z_{33}|}{|Z_{33}|^2 - |Z_{23}|^2} \right) \\
\sigma_1 &\equiv \arg(Z_{22}^* Z_{23} + Z_{23}^* Z_{33}) \\
\sigma_2 &\equiv \arg\{Z_{22} \cos^2 \chi + Z_{33} \sin^2 \chi e^{-2i\sigma_1} - Z_{23} \sin 2\chi e^{-i\sigma_1}\}
\end{aligned} \tag{49}$$

The eigenvalues of Z are

$$m_2 = Z_{22} \cos^2 \chi e^{-2i\sigma_2} + Z_{33} \sin^2 \chi e^{-2i(\sigma_1+\sigma_2)} - Z_{23} \sin 2\chi e^{-i(\sigma_1+2\sigma_2)} \tag{50}$$

and

$$m_3 = Z_{22} \cos^2 \chi e^{-2i\sigma_2} + Z_{33} \sin^2 \chi e^{-2i(\sigma_1+\sigma_2)} + Z_{23} \sin 2\chi e^{-i(\sigma_1+2\sigma_2)}. \tag{51}$$

The PMNS matrix corresponds with the product of V and K in the base of diagonalized charged lepton mass matrix,

$$V_{PMNS} = VK. \tag{52}$$

$$\begin{aligned}
V_{PMNS}^\dagger m_{eff} V_{PMNS}^* &= (VK)^\dagger (-U X U^t) (VK)^* \\
&= \begin{pmatrix} 0 & 0 & 0 \\ 0 & m_2 & 0 \\ 0 & 0 & m_3 \end{pmatrix}.
\end{aligned} \tag{53}$$

4 Classification of four-zero textures

The configuration of the four-zero texture in three by three Dirac mass matrix \mathcal{U} has ${}_9C_4 = 126$ different patterns. We classify them into seven classes by imposing conditions in this section.

Let us introduce the matrices Q and P .

$$\begin{aligned}
P, Q &= \begin{pmatrix} 1 & 0 & 0 \\ 0 & 1 & 0 \\ 0 & 0 & 1 \end{pmatrix}, \begin{pmatrix} 1 & 0 & 0 \\ 0 & 0 & 1 \\ 0 & 1 & 0 \end{pmatrix}, \begin{pmatrix} 0 & 1 & 0 \\ 1 & 0 & 0 \\ 0 & 0 & 1 \end{pmatrix}, \\
&\begin{pmatrix} 0 & 1 & 0 \\ 0 & 0 & 1 \\ 1 & 0 & 0 \end{pmatrix}, \begin{pmatrix} 0 & 0 & 1 \\ 1 & 0 & 0 \\ 0 & 1 & 0 \end{pmatrix}, \begin{pmatrix} 0 & 0 & 1 \\ 0 & 1 & 0 \\ 1 & 0 & 0 \end{pmatrix}.
\end{aligned} \tag{54}$$

We define that P is always multiplied on \mathcal{U} from right side and Q from left side. P and Q correspond to replacements of column and row components respectively. We classify the configurations of Dirac mass matrix on condition that any textures in a same class are related to each other by means of the replacements of row and column components. If we only consider the position of zero and non-zero elements on the Dirac mass matrix, the configuration between a texture \mathcal{U} and another texture \mathcal{U}' in the same class is expressed as

$$\mathcal{U}' = Q\mathcal{U}P. \tag{55}$$

Taking the suitable P and Q , any two textures in the same class are related to each other by Eq.(55). P replaces the column components of \mathcal{U} multiplied from the right side. Q replaces the row components of \mathcal{U} multiplied from the left side.

The texture Eq.(35) taken as an example in section 3.2 shall belong to the class (I). All textures in the class (I) are

$$\begin{aligned}
& \begin{pmatrix} * & * & * \\ * & 0 & 0 \\ 0 & * & 0 \end{pmatrix}, \begin{pmatrix} * & * & * \\ * & 0 & 0 \\ 0 & 0 & * \end{pmatrix}, \begin{pmatrix} * & * & * \\ 0 & * & 0 \\ * & 0 & 0 \end{pmatrix}, \begin{pmatrix} * & * & * \\ 0 & * & 0 \\ 0 & 0 & * \end{pmatrix}, \begin{pmatrix} * & * & * \\ 0 & 0 & * \\ * & 0 & 0 \end{pmatrix}, \begin{pmatrix} * & * & * \\ 0 & 0 & * \\ 0 & * & 0 \end{pmatrix} \\
& \begin{pmatrix} 0 & * & 0 \\ * & * & * \\ * & 0 & 0 \end{pmatrix}, \begin{pmatrix} 0 & 0 & * \\ * & * & * \\ * & 0 & 0 \end{pmatrix}, \begin{pmatrix} * & 0 & 0 \\ * & * & * \\ 0 & * & 0 \end{pmatrix}, \begin{pmatrix} 0 & 0 & * \\ * & * & * \\ 0 & * & 0 \end{pmatrix}, \begin{pmatrix} * & 0 & 0 \\ * & * & * \\ 0 & 0 & * \end{pmatrix}, \begin{pmatrix} 0 & * & 0 \\ * & * & * \\ 0 & 0 & * \end{pmatrix} \\
& \begin{pmatrix} * & 0 & 0 \\ 0 & * & 0 \\ * & * & * \end{pmatrix}, \begin{pmatrix} * & 0 & 0 \\ 0 & 0 & * \\ * & * & * \end{pmatrix}, \begin{pmatrix} 0 & * & 0 \\ * & 0 & 0 \\ * & * & * \end{pmatrix}, \begin{pmatrix} 0 & * & 0 \\ 0 & 0 & * \\ * & * & * \end{pmatrix}, \begin{pmatrix} 0 & 0 & * \\ * & 0 & 0 \\ * & * & * \end{pmatrix}, \begin{pmatrix} 0 & 0 & * \\ 0 & * & 0 \\ * & * & * \end{pmatrix},
\end{aligned} \tag{56}$$

where * stands for the non-zero element. The number of combinations multiplying P and Q is 36. However, the class (I) has 18 textures because of overlaps. All 126 textures can be classified into seven independent classes (I)-(VII) without exception. We define them briefly and give one representation as an example texture for each class.

(I) There is only one row component in which all elements are non-zero, and rank $\mathcal{U} = 3$.

$$\begin{pmatrix} * & * & * \\ * & 0 & 0 \\ 0 & * & 0 \end{pmatrix} \dots 18 \text{ patterns} \tag{57}$$

(II) There is only one column component in which all elements are non-zero, and rank $\mathcal{U} = 3$.

$$\begin{pmatrix} * & * & 0 \\ * & 0 & * \\ * & 0 & 0 \end{pmatrix} \dots 18 \text{ patterns} \tag{58}$$

(III) There are one row and column components in which two elements are zero, and the common element on the both of such row and column is zero. Besides, we require that rank $\mathcal{U} = 3$.

$$\begin{pmatrix} * & 0 & 0 \\ * & * & 0 \\ 0 & * & * \end{pmatrix} \dots 36 \text{ patterns} \tag{59}$$

(IV) There is only one column component in which all elements are zero.

$$\begin{pmatrix} * & * & 0 \\ * & * & 0 \\ * & 0 & 0 \end{pmatrix} \dots 18 \text{ patterns} \tag{60}$$

(V) There is only one row component in which all elements are zero.

$$\begin{pmatrix} * & * & * \\ * & * & 0 \\ 0 & 0 & 0 \end{pmatrix} \dots 18 \text{ patterns} \tag{61}$$

(VI) There is one row component and one column component in which all elements are non-zero.

$$\begin{pmatrix} * & * & * \\ * & 0 & 0 \\ * & 0 & 0 \end{pmatrix} \dots 9 \text{ patterns} \quad (62)$$

(VII) There are one row and column components in which two elements are zero, and the common element on the both of such row and column is not zero.

$$\begin{pmatrix} * & 0 & 0 \\ 0 & * & * \\ 0 & * & * \end{pmatrix} \dots 9 \text{ patterns} \quad (63)$$

Textures of class (I), (II), (III), (VI) and (VII) are expressed four parameters; two angles θ_1, θ_2 and two phases ϕ_1, ϕ_2 . Textures of class (IV) are expressed five parameters; three angles $\theta_1, \theta_2, \theta_3$ and two phases ϕ_1, ϕ_2 as shown in Eq.(36). Textures of class (IV) are expressed five parameters; two angles θ_1, θ_2 and three phases ϕ_1, ϕ_2, ϕ_3 as shown in Eq.(37).

This classification is useful to investigate the number of non-zero neutrino mass eigenvalues and the existence of CP breaking phase for each class. Class (V), (VI), and (VII) lead to that $\Delta = 0$. We do not consider those three classes in order to explain the CP violation in the neutrino sector. A texture with $\det \mathcal{U} = 0$ causes at least one zero mass eigenvalue of m_{eff} . Class (IV), (V), and (VI), whose rank is 2, produce a zero mass eigenvalue for neutrino. Although the existence of one massless neutrino is still allowed at present, this class (IV) leads to the same effective Majorana mass matrix as that of the seesaw model with two right handed neutrinos. Taking more general assumption that all three mass eigenvalues are non-zero, we do not consider it. From the reasons above, we adopt three classes (I), (II) and (III). All textures to be investigated in later sections are parametrized in terms of two angles θ_1, θ_2 and two phases ϕ_1, ϕ_2 . We summarize the number of neutrino mass eigenvalues and the existence of CP breaking phase for each classes in Table 1.

5 Numerical analysis

In this section, we perform the numerical analysis of four-zero texture. We have adopted three classes as acceptable models. There are still 72 textures to be analyzed. Classes (I), (II) and (III) are more classified into 3, 3 and 6 subclasses respectively according to the replacement of column components. Each subclass includes 6 textures. In section 5.1, we outline the method of numerical analysis. In section 5.2, we define the sub-classification and explain how is it useful for numerical calculation. In section 5.3, we show some concrete results of the numerical calculation. We specially focus on the correlations among CP phases, since they are predictable parameters of physics.

5.1 How to perform the numerical analysis

The m_{eff} of four-zero texture model is parametrized with three mass scales $X_i (i = 1 \sim 3)$, two angles θ_1, θ_2 and two phases ϕ_1, ϕ_2 as shown in Eq.(32) and

Table 1: The number of neutrino mass eigenvalues and the existence of CP breaking phase for each class

class	represent texture	Number of different textures	Number of non-zero mass eigenvalues	Δ
(I)	$\begin{pmatrix} * & * & * \\ * & 0 & 0 \\ 0 & * & 0 \end{pmatrix}$	18	3	non-0
(II)	$\begin{pmatrix} * & * & 0 \\ * & 0 & * \\ * & 0 & 0 \end{pmatrix}$	18	3	non-0
(III)	$\begin{pmatrix} * & 0 & 0 \\ * & * & 0 \\ 0 & * & * \end{pmatrix}$	36	3	non-0
(IV)	$\begin{pmatrix} * & * & 0 \\ * & * & 0 \\ * & 0 & 0 \end{pmatrix}$	18	2	non-0
(V)	$\begin{pmatrix} * & * & * \\ * & * & 0 \\ 0 & 0 & 0 \end{pmatrix}$	18	2	0
(VI)	$\begin{pmatrix} * & * & * \\ * & 0 & 0 \\ * & 0 & 0 \end{pmatrix}$	9	2	0
(VII)	$\begin{pmatrix} * & 0 & 0 \\ 0 & * & * \\ 0 & * & * \end{pmatrix}$	9	3	0

Eq.(35). The m_{eff} satisfies the following eigenvalue equation [22].

$$\det(m_{\text{eff}} m_{\text{eff}}^\dagger - \lambda I) = 0. \quad (64)$$

I is the three by three unit matrix and eigenvalues λ 's correspond to mass squares. The m_{eff} is a complex symmetric matrix. We have to make an Hermite matrix $m_{\text{eff}} m_{\text{eff}}^\dagger$ to solve its eigenvalue equation. Eq.(64) is identical to the following three algebraic equations,

$$\text{tr}(m_{\text{eff}} m_{\text{eff}}^\dagger) = m_1^2 + m_2^2 + m_3^2, \quad (65)$$

$$\frac{\{\text{tr}(m_{\text{eff}} m_{\text{eff}}^\dagger)\}^2 - \text{tr}\{(m_{\text{eff}} m_{\text{eff}}^\dagger)^2\}}{2} = m_1^2 m_2^2 + m_2^2 m_3^2 + m_3^2 m_1^2, \quad (66)$$

$$\det(m_{\text{eff}} m_{\text{eff}}^\dagger) = m_1^2 m_2^2 m_3^2, \quad (67)$$

where $m_i (i = 1 \sim 3)$ are mass eigenvalues of neutrinos. The left-hand side of Eqs.(65) -(67) are written in terms of model parameters: X_i , angles θ_1, θ_2 and phases ϕ_1, ϕ_2 . The numerical values of the right-hand side are fixed with the neutrino mass squared differences for a given value of the lightest neutrino mass and hierarchy (normal or inverted) of neutrino mass spectrum. We randomly generate a set of values for Δm_{sol}^2 and Δm_{atm}^2 within 3 standard deviations from the mean of the experimental values in the Table 1 of Ref.[25]. We allocate the

value of the lightest neutrino mass $m_1(m_3)$ for normal (inverted) hierarchical case from 0 eV to its upper bound 0.046 eV. Assigning the numerical values for angles θ_1 , θ_2 and phases ϕ_1 and ϕ_2 randomly from $-\pi$ to π , since they are not restricted, Eqs.(65) -(67) become then three equations as for three X s. We make a computer solve them and gather the real positive solutions of X s and accompanying allocated parameters; θ_1 , θ_2 , ϕ_1 , ϕ_2 , $\Delta m_{\text{sol.}}^2$, $\Delta m_{\text{atm.}}^2$ and $m_1(m_3)$.

m_{eff} is reconstructed in terms of the numerically determined parameters and solved X s. By using the obtained m_{eff} , we compute mixing angles $\theta_{12}, \theta_{23}, \theta_{13}$ and three CP phases $\delta, \alpha_{21}, \alpha_{31}$. If all three mixing angles are within 3 standard deviations from the mean of the experimental values in the Table 1 of Ref.[25], we take such parameters as a possible model. CP phases and the correlations among them can be predictions. We collect the set of the parameters which produce the appropriate mixing angles by repeating this procedure. In principle, the procedure explained above can be applied to all the textures in class (I), (II) and (III). However, we do not have to repeat the procedure for all textures in a class individually. By using some relations of parameters of two different textures in a class, we can save labor to examine them.

5.2 Sub-classification

The configurations of all textures in a specific class are related to each other by exchanging their column and rows. Taking the suitable P and Q , any two textures in the same class are related to each other by Eq.(55). Let us define X' as

$$X' = P^t X P. \quad (68)$$

The m'_{eff} , which is constructed by \mathcal{U}' in Eq.(55) and X' in Eq.(68) through the definition Eq.(32) in stead of \mathcal{U} and X , is expressed in terms of the original m_{eff} and Q .

$$\begin{aligned} m'_{\text{eff}} &= -\mathcal{U}' X' (\mathcal{U}')^t \\ &= Q m_{\text{eff}} Q^T. \end{aligned} \quad (69)$$

The m'_{eff} satisfies the same constraints Eqs.(65)-(67). We introduce a unitary matrix V which diagonalizes $m_{\text{eff}} m_{\text{eff}}^\dagger$,

$$V^\dagger (m_{\text{eff}} m_{\text{eff}}^\dagger) V = \begin{pmatrix} m_1^2 & 0 & 0 \\ 0 & m_2^2 & 0 \\ 0 & 0 & m_3^2 \end{pmatrix}, \quad (70)$$

while the mixing matrix V' which diagonalizes $m'_{\text{eff}} (m'_{\text{eff}})^\dagger$ is

$$V' = Q V. \quad (71)$$

If we once do the analysis as for a texture \mathcal{U} , we obtain another m'_{eff} by arranging the elements of m_{eff} . The other effective mass matrices in the same class are calculated out without solving extra eigenvalue equations. Since it reduces the processing loads of solving eigenvalue equations, the method is much more efficient for numerical analysis.

Next, we investigate the classification of Eq.(57)-(58) in detail. In each class of (I)-(III), we further classify the textures into subclasses. The 18 textures

of the class (I) are classified into three subclasses called class (I)-A, (I)-B and (I)-C. The Dirac matrices which belong to each subclass have a row with all non-zero elements. In matrices of class (I)-A, all elements of the first row do not vanish and in class (I)-B, all of the elements of the second row does not vanish. In class (I)-C, all of them in the third row have non-zero values. Let us define subclasses of Dirac matrices called as (I)-B and (I)-C. The matrices in (I)-B are obtained by multiplying those in subclass (I)-A by

$$Q = \begin{pmatrix} 0 & 0 & 1 \\ 1 & 0 & 0 \\ 0 & 1 & 0 \end{pmatrix}. \quad (72)$$

In the same way, the matrices in (I)-C are obtained by multiplying those in (I)-A by matrix

$$Q = \begin{pmatrix} 0 & 1 & 0 \\ 0 & 0 & 1 \\ 1 & 0 & 0 \end{pmatrix}. \quad (73)$$

We summarize all textures of (I)-A, (I)-B and (I)-C in Table 2. These sub-

(I)-A	$\begin{pmatrix} * & * & * \\ * & 0 & 0 \\ 0 & * & 0 \end{pmatrix}, \begin{pmatrix} * & * & * \\ * & 0 & 0 \\ 0 & 0 & * \end{pmatrix}, \begin{pmatrix} * & * & * \\ 0 & * & 0 \\ * & 0 & 0 \end{pmatrix},$ $\begin{pmatrix} * & * & * \\ 0 & * & 0 \\ 0 & 0 & * \end{pmatrix}, \begin{pmatrix} * & * & * \\ 0 & 0 & * \\ * & 0 & 0 \end{pmatrix}, \begin{pmatrix} * & * & * \\ 0 & 0 & * \\ 0 & * & 0 \end{pmatrix}$
(I)-B	$\begin{pmatrix} 0 & * & 0 \\ * & * & * \\ * & 0 & 0 \end{pmatrix}, \begin{pmatrix} 0 & 0 & * \\ * & * & * \\ * & 0 & 0 \end{pmatrix}, \begin{pmatrix} * & 0 & 0 \\ * & * & * \\ 0 & * & 0 \end{pmatrix},$ $\begin{pmatrix} 0 & 0 & * \\ * & * & * \\ * & * & * \end{pmatrix}, \begin{pmatrix} * & 0 & 0 \\ * & * & * \\ 0 & 0 & * \end{pmatrix}, \begin{pmatrix} * & * & * \\ 0 & * & 0 \\ 0 & 0 & * \end{pmatrix}$
(I)-C	$\begin{pmatrix} * & 0 & 0 \\ 0 & * & 0 \\ * & * & * \end{pmatrix}, \begin{pmatrix} * & 0 & 0 \\ 0 & 0 & * \\ * & * & * \end{pmatrix}, \begin{pmatrix} 0 & * & 0 \\ * & 0 & 0 \\ * & * & * \end{pmatrix},$ $\begin{pmatrix} 0 & * & 0 \\ 0 & 0 & * \\ * & * & * \end{pmatrix}, \begin{pmatrix} * & 0 & 0 \\ * & * & * \\ * & * & * \end{pmatrix}, \begin{pmatrix} 0 & * & 0 \\ 0 & * & 0 \\ * & * & * \end{pmatrix}$

Table 2: The subclasses of class (I)

classes can be related to each other by applying the permutation matrix Q on \mathcal{U} . By multiplying the permutation matrix P on a Dirac matrix \mathcal{U} in each subclass,

$$\mathcal{U}'' = \mathcal{U}P, \quad (74)$$

one can generate all six different matrices which belong to the same subclass. Eq.(74) corresponds to the specific case of Eq.(55) such that Q is identical to the unit matrix, and indicates the replacements of columns. The effective matrix constructed from (\mathcal{U}'', X') is the same as that from (\mathcal{U}, X) and it is therefore diagonalized by the same matrix V . If one finds real solutions of Eq.(64) for X s

and if obtained mixing angles are consistent with the experimental results from neutrino oscillation, it is confirmed that the other 5 textures also have model parameters satisfying with the constraints from mass eigenvalues and mixing angles. On the other hand, if one texture does not give any correct mixing angles, there is no hope that the others would realize the experimental results either.

Any subclass has 6 textures related by Eq.(74). We carry out the same manner of classification for class (II) as we have done for class (I). Class (III) contains 36 textures, therefore it is categorized into 6 subclasses from (III)-A to (III)-F. We arrange the subclasses in Table 3, by picking up one representation for each subclass.

	class (I)	class (II)	class (III)
A	$\begin{pmatrix} * & * & * \\ * & 0 & 0 \\ 0 & * & 0 \\ 0 & * & 0 \end{pmatrix}$	$\begin{pmatrix} * & * & 0 \\ * & 0 & * \\ * & 0 & 0 \\ * & 0 & 0 \end{pmatrix}$	$\begin{pmatrix} * & 0 & 0 \\ * & * & 0 \\ 0 & * & * \\ 0 & * & * \end{pmatrix}$
B	$\begin{pmatrix} * & * & * \\ * & 0 & 0 \\ * & 0 & 0 \\ * & 0 & 0 \end{pmatrix}$	$\begin{pmatrix} * & * & 0 \\ * & * & 0 \\ * & 0 & * \\ * & 0 & * \end{pmatrix}$	$\begin{pmatrix} * & 0 & 0 \\ * & * & 0 \\ * & * & 0 \\ 0 & * & * \end{pmatrix}$
C	$\begin{pmatrix} * & * & * \\ 0 & * & 0 \\ * & * & * \\ * & * & * \end{pmatrix}$	$\begin{pmatrix} * & * & 0 \\ * & 0 & * \\ * & 0 & 0 \\ * & * & 0 \end{pmatrix}$	$\begin{pmatrix} * & * & 0 \\ 0 & * & * \\ * & 0 & 0 \\ * & 0 & 0 \end{pmatrix}$
D			$\begin{pmatrix} * & * & 0 \\ * & 0 & 0 \\ 0 & * & * \\ * & 0 & 0 \end{pmatrix}$
E			$\begin{pmatrix} 0 & * & * \\ * & * & 0 \\ 0 & * & * \\ * & * & 0 \end{pmatrix}$
F			$\begin{pmatrix} 0 & * & * \\ * & * & 0 \\ * & * & 0 \\ * & 0 & 0 \end{pmatrix}$

Table 3: The classification of textures such that each subclass has six textures

Since all 6 textures in each subclass numerically produce the same m_{eff} , we can consider these 6 textures as the same model to lead the mass eigenvalues, mixing angles and CP phases. Therefore, it is sufficient to make analysis for one texture out of six. There are only 12 textures to be investigated. In later discussion, we use the name of subclass (I)-A to (III)-F as analyzable models.

5.3 Results

We study the results of numerical calculation. The correlations among model parameters, among mass eigenvalues and among CP phases are shown as Figs.(1-35) in section 5.3.1, as Figs.(36-43) in section 5.3.2 and as Figs.(48-83) in section 5.3.3 respectively. We select concrete results of numerical analysis for subclasses summarized in Table 3 according to normal or inverted hierarchical cases. In Table 4, we show the number of figures which correspond to each subclass. The correlations among CP phases are explained in more detail because they

can be predictions and some of them produces characteristic results, which are comparable with the later discussion in section 6. Neither the cases with few data nor the cases without strong correlations are not shown.

We also comment on the textures which are not consistent with the experimental data. We find that subclasses (I)-A, (III)-C and (III)-D in normal hierarchy case are not consistent with them. The (2,3) and (3,2) elements of the effective mass matrix built only by these textures are equal to zero, namely $(m_{\text{eff}})_{\mu\tau} = (m_{\text{eff}})_{\tau\mu} = 0$. In inverted hierarchy case, only subclass (II)-B does not lead to the experimental data. We note it in Table 4 which subclass does not produce results. In section 6.2.4 and 6.2.5, we explain the reason why these textures are not consistent with the experimental data in context with the zero-texture on m_{eff} .

5.3.1 Correlations among model parameters

To show the characteristic results for model parameters θ_1 , θ_2 , ϕ_1 , ϕ_2 , X_1 , X_2 and X_3 , we select those of subclasses (I)-C(NH) as Figs.(1-5), (III)-A(NH) as Figs.(6-10), (I)-B(IH),(I)-C(IH) as Figs.(11-15), (III)-B(IH) as Figs.(21-25), (III)-E(IH) as Figs.(26-30) and (III)-F(IH) as Figs.(31-35). Correlations of θ_1 vs θ_2 , ϕ_1 vs ϕ_2 , X_1 vs X_2 , X_1 vs X_3 and X_2 vs X_3 are shown for each subclass.

For the correlation between two model angles θ_1 and θ_2 , all subclasses show that the similar distributions of plots symmetrically with respect to the lines $\theta_1 = 0$ and $\theta_2 = 0$. The same pattern is found in all four quadrant in the $\theta_1 - \theta_2$ plane. The plots are distributed elliptically in a quadrant. The shape and spread of those differ depending on the subclasses. The Fig.11 shows the most clear shape. There are four similar elliptical plots centered on the points $(\theta_1, \theta_2) = (\frac{\pi}{2}, \frac{\pi}{2})$, $(-\frac{\pi}{2}, \frac{\pi}{2})$, $(-\frac{\pi}{2}, -\frac{\pi}{2})$ and $(\frac{\pi}{2}, -\frac{\pi}{2})$. The Fig.31 also show the four similar elliptical plots on the $\theta_1 - \theta_2$ plane. θ_2 is distributed all round from $-\pi$ to π , while θ_1 appears in the restricted range near $\theta_1 = \pm\frac{\pi}{2}$

For the correlation between two model phases ϕ_1 and ϕ_2 , some subclasses show the similar characteristic shapes. Fig.7, Fig.12, Fig.22 and Fig.27 shows the similar net-like distribution. On the other hand, Fig.2, Fig.17 and Fig.32 do not produce such a characteristic pattern of plots. There are no strong correlation between ϕ_1 and ϕ_2 for those three subclasses. ϕ_2 is distributed all around from $-\pi$ to π , while ϕ_1 is restricted in a narrow range. Their distributions are roughly symmetric with respect to the line $\phi_1 = 0$.

For the correlation among model mass-scale parameters X_1 , X_2 and X_3 , show that the most of plots gather in a narrow region and that there are two or three straight lines through the region. This feature is found in all planes of any two X s independent of subclasses. For example, in Fig.10, which gives the correlation between X_2 and X_3 of subclass (III)-A in NH, plots are found in the region $(0.03eV < X_2 < 0.08eV, 0.03eV < X_3 < 0.06eV)$ and some plots are also distributed near the two straight lines $X_2 = X_3$ and $X_3 = 0.03ev$. The gradients of straight lines depend on subclasses. Some of them are parallel to $X_i = 0 (i = 1, 2, 3)$.

5.3.2 Correlations among mass eigenvalues

We select the results of subclasses (I)-C(NH) as Figs.(36-39), (III)-A(NH) as Figs.(40-43) and (I)-B(IH) as Fig.(44-Fig.47). Correlations of m_1 vs m_2 , m_1 vs

	Correlations among model parameters		Correlations among mass eigenvalues		Correlations among CP phases	
	NH	IH	NH	IH	NH	IH
(I)-A	(no result)		(no result)		(no result)	
(I)-B		Fig.11 Fig.12 Fig.13 Fig.14 Fig.15		Fig.44 Fig.45 Fig.46 Fig.47		Fig.60 Fig.61 Fig.62 Fig.63
(I)-C	Fig.1 Fig.2 Fig.3 Fig.4 Fig.5	Fig.16 Fig.17 Fig.18 Fig.19 Fig.20	Fig.36 Fig.37 Fig.38 Fig.39			Fig.64 Fig.65 Fig.66 Fig.67
(II)-A					Fig.52 Fig.53 Fig.54 Fig.55	
(II)-B		(no result)		(no result)		(no result)
(II)-C					Fig.56 Fig.57 Fig.58 Fig.59	
(III)-A	Fig.6 Fig.7 Fig.8 Fig.9 Fig.10		Fig.40 Fig.41 Fig.42 Fig.43		Fig.48 Fig.49 Fig.50 Fig.51	Fig.68 Fig.69 Fig.70 Fig.71
(III)-B		Fig.21 Fig.22 Fig.23 Fig.24 Fig.25				Fig.72 Fig.73 Fig.74 Fig.75
(III)-C	(no result)		(no result)		(no result)	
(III)-D	(no result)		(no result)		(no result)	
(III)-E		Fig.26 Fig.27 Fig.28 Fig.29 Fig.30				Fig.76 Fig.77 Fig.78 Fig.79
(III)-F		Fig.31 Fig.32 Fig.33 Fig.34 Fig.35				Fig.80 Fig.81 Fig.82 Fig.83

Table 4: Figure numbers to which subclasses correspond

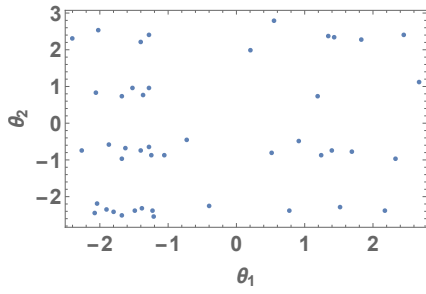


Figure 1: θ_1 vs θ_2 (I)-C in NH

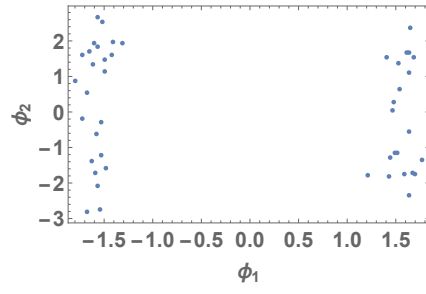


Figure 2: ϕ_1 vs ϕ_2 (I)-C in NH

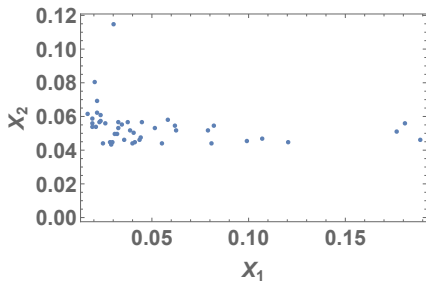


Figure 3: X_1 vs X_2 (I)-C in NH

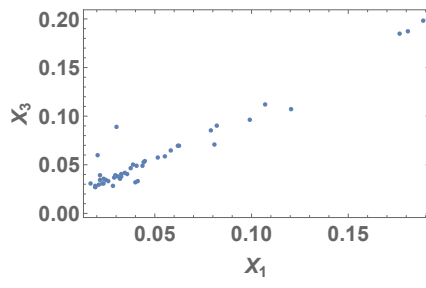


Figure 4: X_1 vs X_3 (I)-C in NH

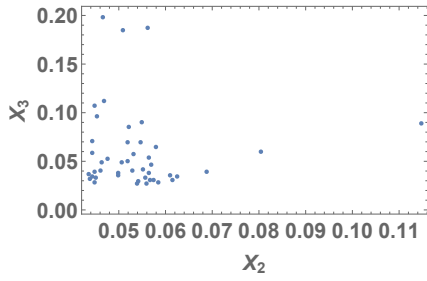


Figure 5: X_2 vs X_3 (I)-C in NH

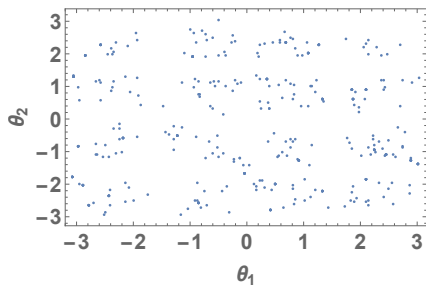


Figure 6: θ_1 vs θ_2 (III)-A in NH

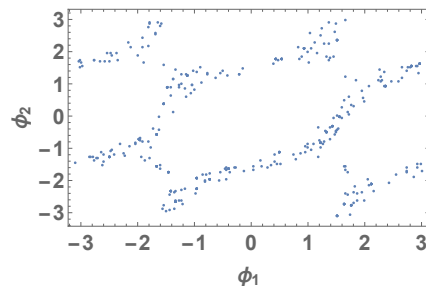


Figure 7: ϕ_1 vs ϕ_2 (III)-A in NH

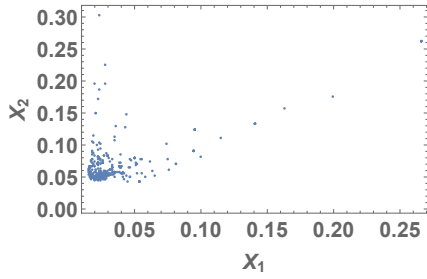


Figure 8: X_1 vs X_2 (III)-A in NH

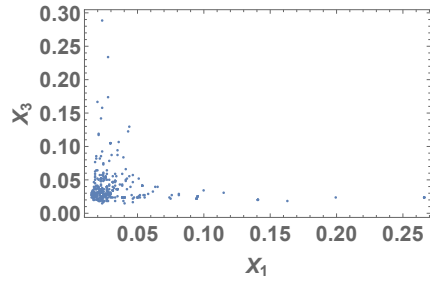


Figure 9: X_1 vs X_3 (III)-A in NH

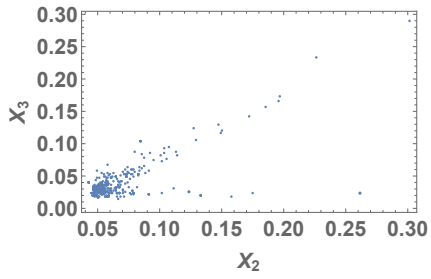


Figure 10: X_2 vs X_3 (III)-A in NH

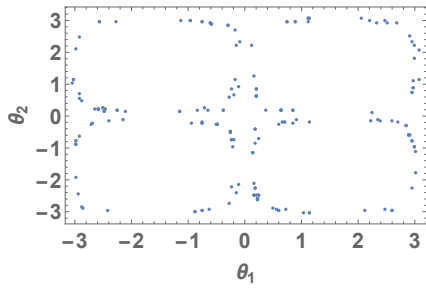


Figure 11: θ_1 vs θ_2 (I)-B in IH

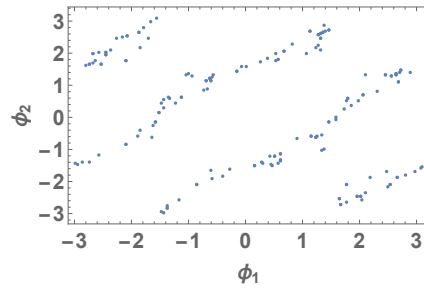


Figure 12: ϕ_1 vs ϕ_2 (I)-B in IH

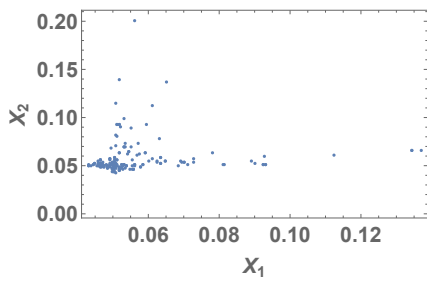


Figure 13: X_1 vs X_2 (I)-B in IH

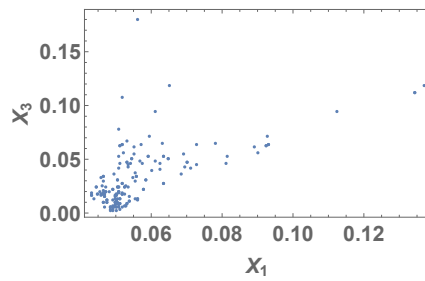


Figure 14: X_1 vs X_3 (I)-B in IH

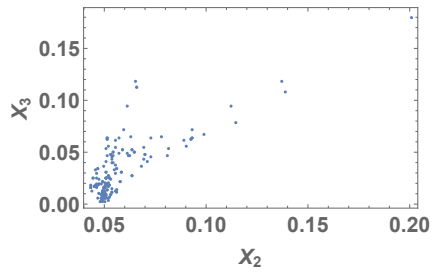


Figure 15: X_2 vs X_3 (I)-B in IH

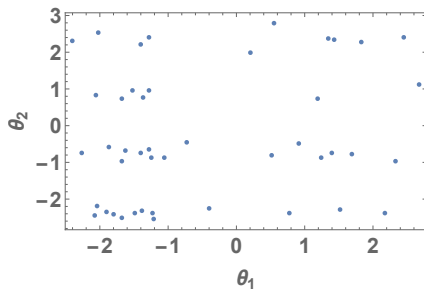


Figure 16: θ_1 vs θ_2 (I)-C in IH

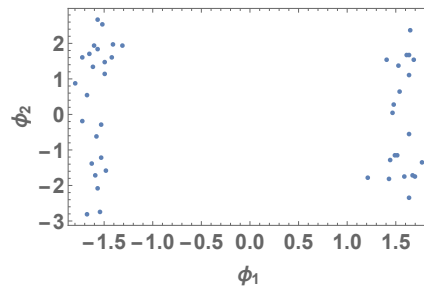


Figure 17: ϕ_1 vs ϕ_2 (I)-C in IH

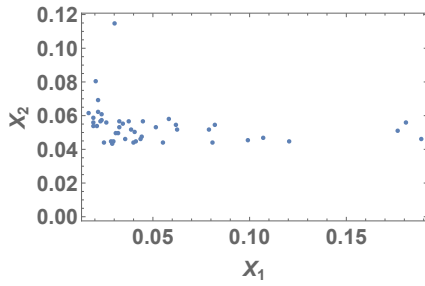


Figure 18: X_1 vs X_2 (I)-C in IH

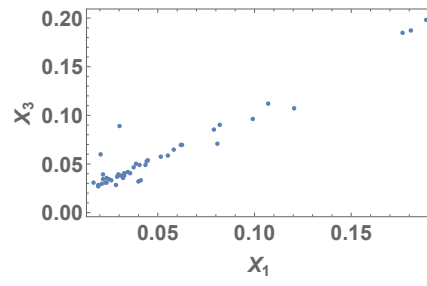


Figure 19: X_1 vs X_3 (I)-C in IH

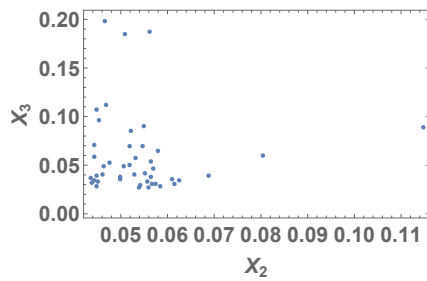


Figure 20: X_2 vs X_3 (I)-C in IH

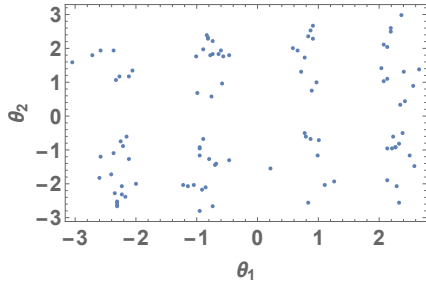


Figure 21: θ_1 vs (III)-B in IH

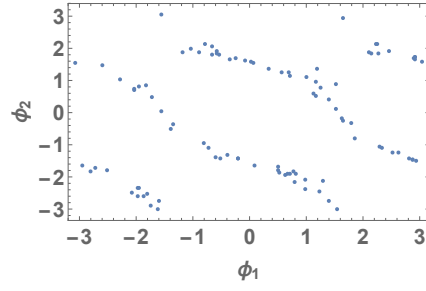


Figure 22: ϕ_1 vs (III)-B in IH

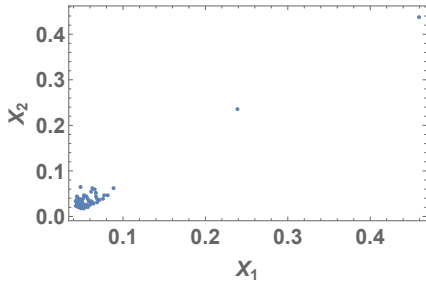


Figure 23: X_1 vs X_2 (III)-B in IH

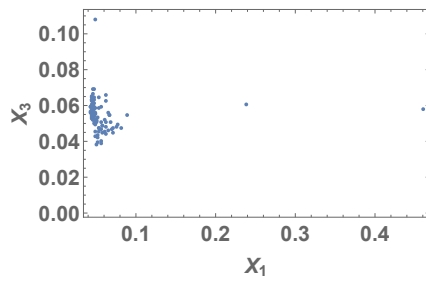


Figure 24: X_1 vs X_3 (III)-B in IH

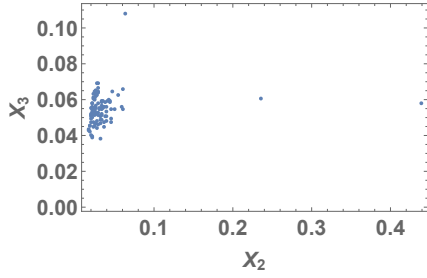


Figure 25: X_2 vs X_3 (III)-B in IH

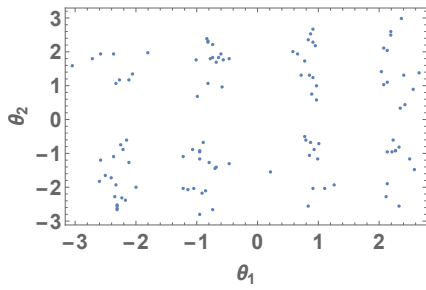


Figure 26: θ_1 vs θ_2 (III)-E in IH

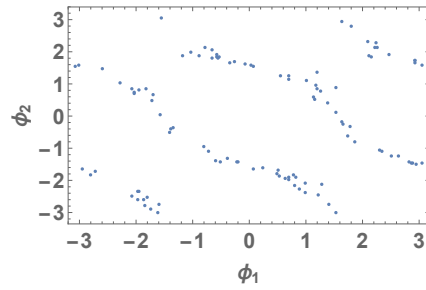


Figure 27: ϕ_1 vs ϕ_2 (III)-E in IH

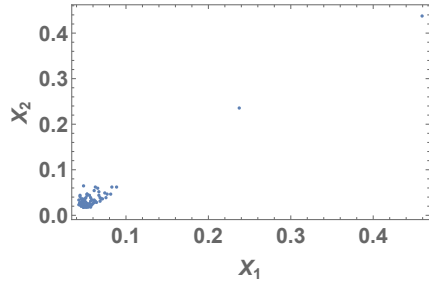


Figure 28: X_1 vs X_2 (III)-E in IH

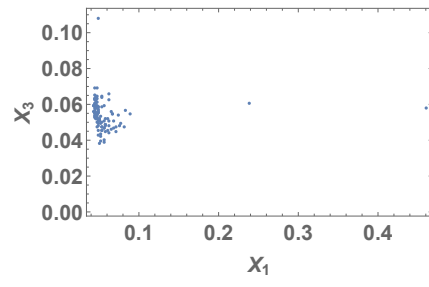


Figure 29: X_1 vs X_3 (III)-E in IH

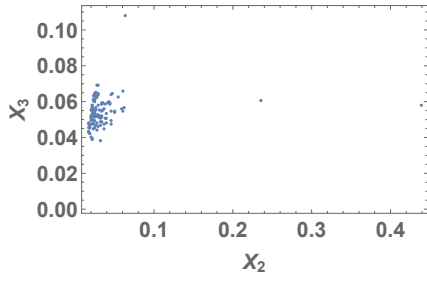


Figure 30: X_2 vs X_3 (III)-E in IH

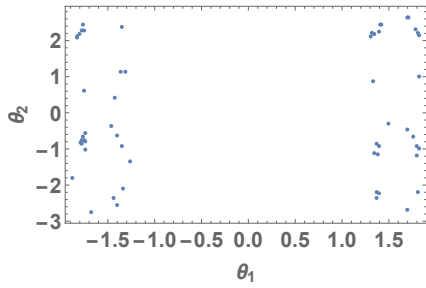


Figure 31: θ_1 vs θ_2 (III)-F in IH

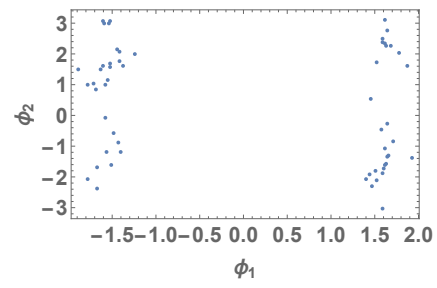


Figure 32: ϕ_1 vs ϕ_2 (III)-F in IH

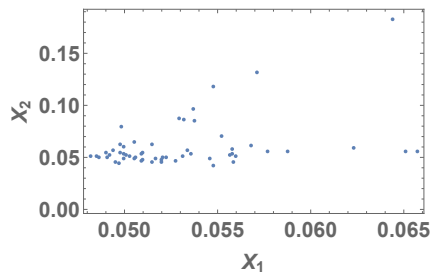


Figure 33: X_1 vs X_2 (III)-F in IH

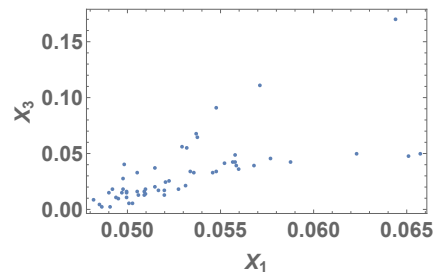


Figure 34: X_1 vs X_3 (III)-F in IH

m_3, m_2 vs m_3 and the lightest neutrino mass $m_1(m_3)$ vs $|m_{ee}|$ are shown.

For the correlations among mass eigenvalues m_1, m_2 and m_3 , one find that two of them are related to positive correlation. The plots on the (m_1, m_2) planes in Fig.(36), Fig.(40) and Fig.(44) form a thin linear because of the small value of $\Delta m_{sol.}$ independently of hierarchies.

The cases (I)-C in NH and (I)-B in IH, in Fig.(39) and Fig.(47) respectively, show the clear correlation that $|m_{ee}|$ is proportional to the lightest neutrino mass $m_1(m_2)$. On the contrary, the case (III)-A in NH, in Fig.(43), does not show any strong correlation between m_1 and $|m_{ee}|$.

5.3.3 Correlations among CP phases

We study the correlations among CP violating phases δ, α_{21} , and α_{31} . We select the results of subclasses (III)-A(NH) as Figs.(48-50), (II)-A(NH) as Figs.(52-54), (II)-C(NH) as Figs.(56-58), (I)-B(IH) as Figs.(60-63), (I)-C(IH) as Figs.(64-67), (III)-A(IH) as Figs.(68-71), (III)-B(IH) as Figs.(72-75), (III)-E(IH) as Figs.(76-79), and (III)-F(IH) as Figs.(80-83), We first show the Correlations among CP phases for normal hierarchical case. For subclass (III)-A, whose correlation is shown in Fig.(48), the dots of (δ, α_{21}) are distributed in a belt on a diagonal line from one corner to the opposite side. Some dots are also found near the other corners. Fig.(52) shows the correlation for the subclass (II)-A. δ takes any values form $-\pi$ to π , while α_{21} appears near the value of 0 independent of δ . In subclass (II)-C in Fig.(56), α_{21} is roughly proportional to $-\delta$ in a range where both α_{21} and δ lie from -1 to 1. Strong correlation is not found outside the range.

Then, we mention the inverted hierarchical case. There is also a characteristic relation between the Dirac CP phase δ and one of the Majorama phases α_{21} in subclasses (I)-B,(I)-C, (III)-A, (III)-B, (III)-E and (III)-F. Their Dirac CP phase δ and the Majorama phase α_{21} are found in the restricted range. In these cases, we do not find no point near $\delta = 0$. The sign of the product of δ and α_{21} is determined by the subclasses. For (I)-C in Fig.(64), for (III)-A in Fig.(68) and for (III)-E in Fig.(76), the plotted points (δ, α_{21}) are predicted only in the second and fourth quadrant. For (I)-B in Fig.(60), for (III)-B in Fig.(72) and for (III)-F in Fig.(80), they are predicted only in the first and third quadrant. The absolute value of α_{21} in (III)-B in Fig.(80) is bigger than those of the other three subclasses.

We find a correlation between δ and α_{21} in some subclasses. On the other hand, the other Majorana phase α_{31} seems to have no strong correlation neither with δ nor with α_{21} . We show the figures δ vs α_{31} for the sake of comparison with α_{21} .

6 Analyses with hidden relations among elements of Majorana mass matrix

6.1 Constraints from vanishing elements on m_{eff}

In this section, we make a discussion as for textures on the effective mass matrix. Constructing the effective mass matrices in terms of our four-zero texture model on Dirac mass matrix, they are categorized into 4 cases from the view point of

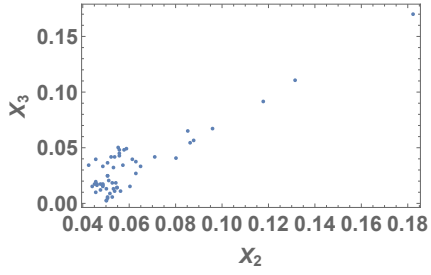


Figure 35: X_2 vs X_3 (III)-F in IH

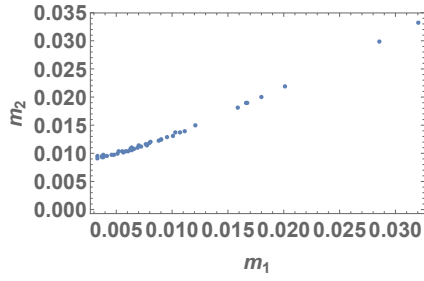


Figure 36: m_1 vs m_2 (I)-C in NH

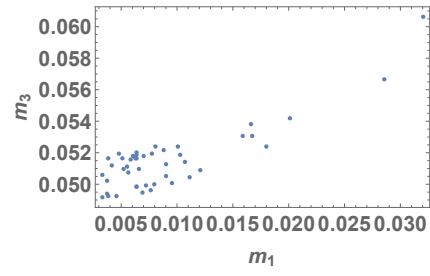


Figure 37: m_1 vs m_3 (I)-C in NH

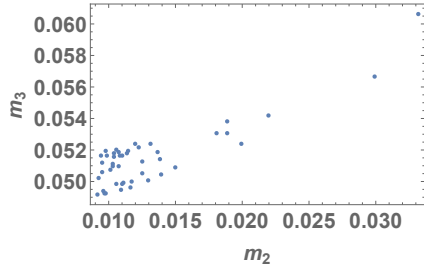


Figure 38: m_2 vs m_3 (I)-C in NH

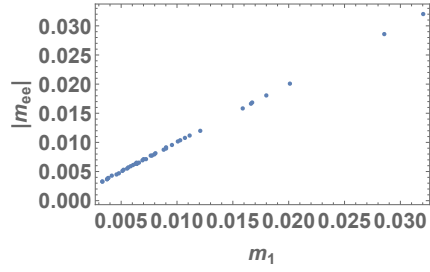


Figure 39: m_1 vs $|m_{ee}|$ (I)-C in NH

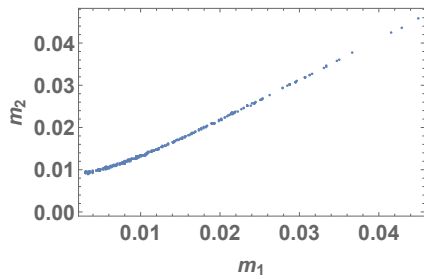


Figure 40: m_1 vs m_2 (III)-A in NH

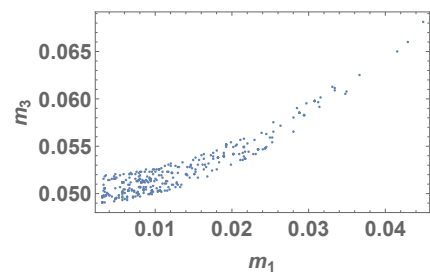


Figure 41: m_1 vs m_3 (III)-A in NH

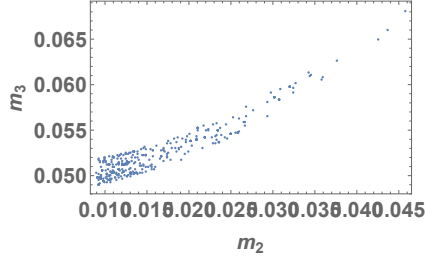


Figure 42: m_2 vs m_3 (III)-A in NH

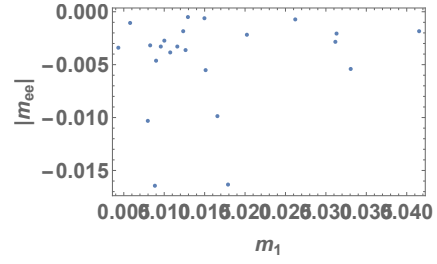


Figure 43: m_1 vs $|m_{ee}|$ (III)-A in NH

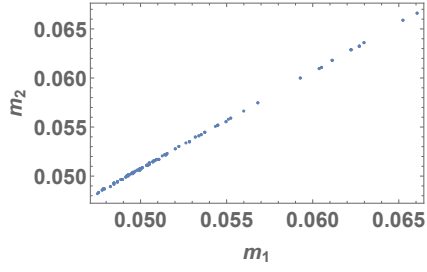


Figure 44: m_1 vs m_2 (I)-B in IH

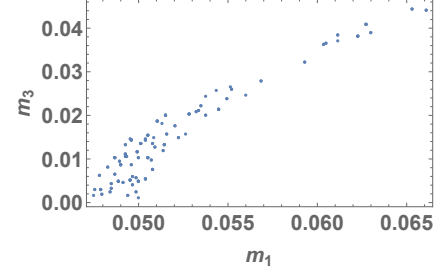


Figure 45: m_1 vs m_3 (I)-B in IH

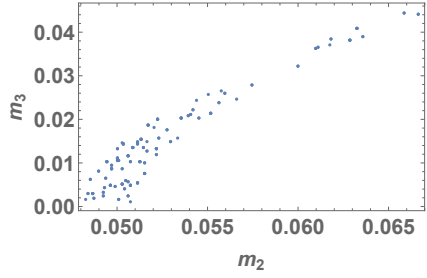


Figure 46: m_2 vs m_3 (I)-B in IH

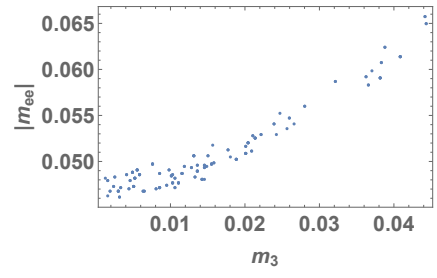


Figure 47: m_3 vs $|m_{ee}|$ (I)-B in IH

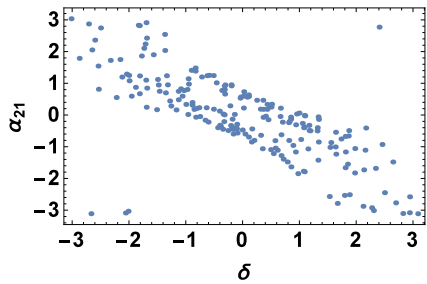


Figure 48: δ vs α_{21} (III)-A in NH

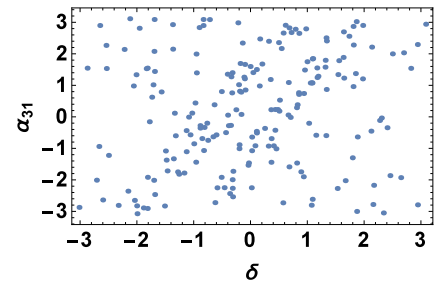


Figure 49: δ vs α_{31} (III)-A in NH

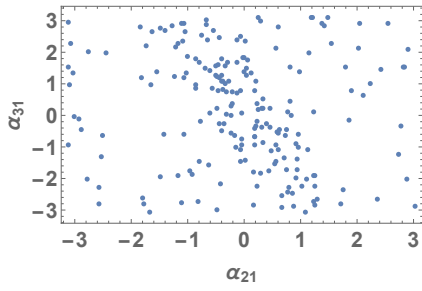


Figure 50: α_{21} vs α_{31} (III)-A in NH

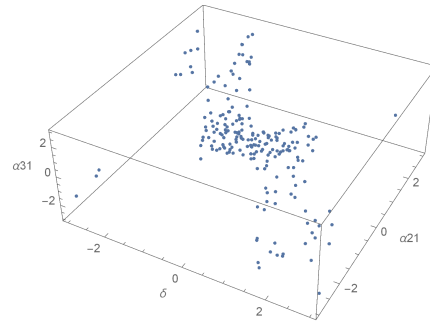


Figure 51: δ vs α_{21} vs α_{31} (III)-A in NH

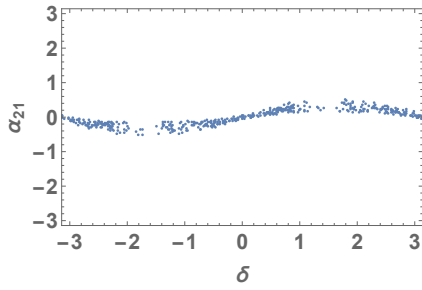


Figure 52: δ vs α_{21} (II)-A in NH

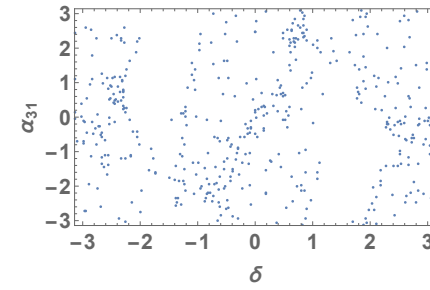


Figure 53: δ vs α_{31} (II)-A in NH

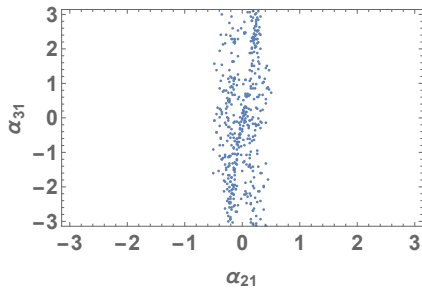


Figure 54: α_{21} vs α_{31} (II)-A in NH

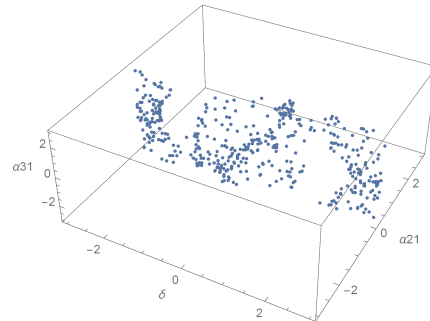


Figure 55: δ vs α_{21} vs α_{31} (II)-A in NH

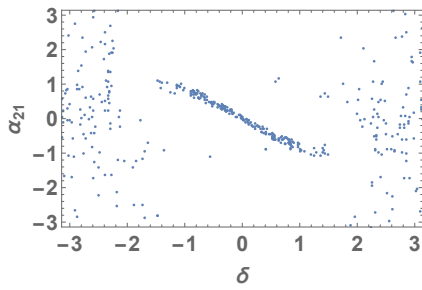


Figure 56: δ vs α_{21} (II)-C in NH

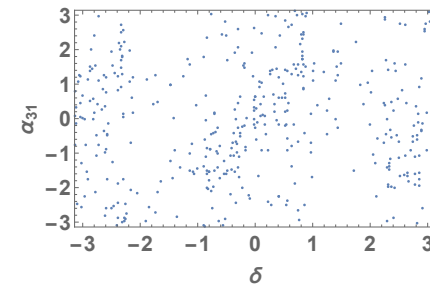


Figure 57: δ vs α_{31} (II)-C in NH

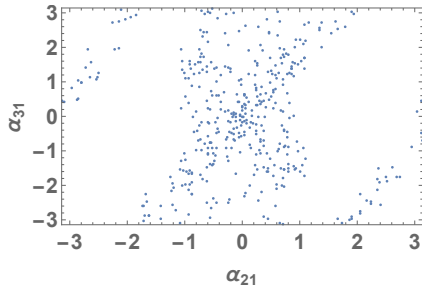


Figure 58: α_{21} vs α_{31} (II)-C in NH

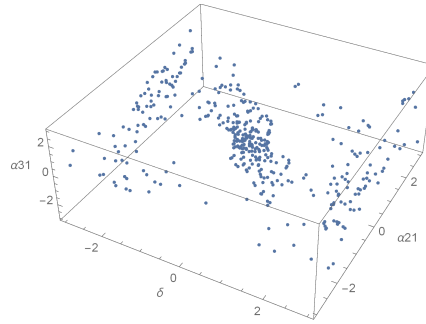


Figure 59: δ vs α_{21} vs α_{31} (II)-C in NH

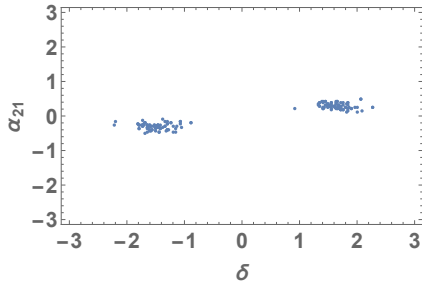


Figure 60: δ vs α_{21} (I)-B in IH

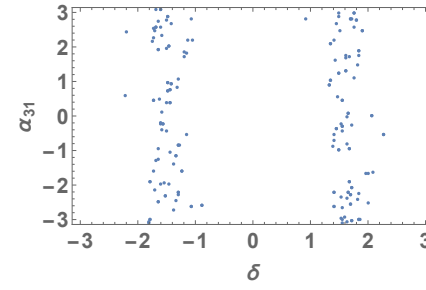


Figure 61: δ vs α_{31} (I)-B in IH

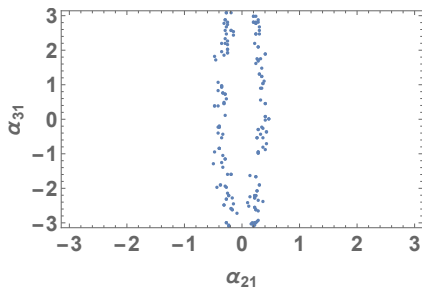


Figure 62: α_{21} vs α_{31} (I)-B in IH

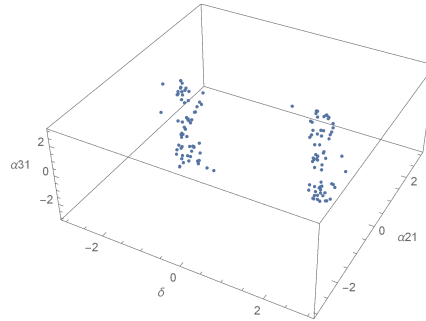


Figure 63: δ vs α_{21} vs α_{31} (I)-B in IH

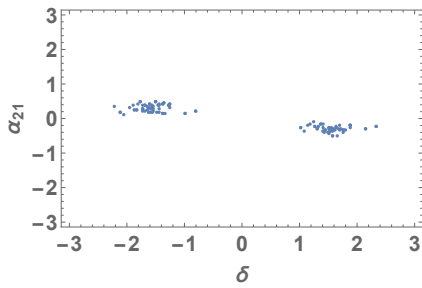


Figure 64: δ vs α_{21} (I)-C in IH

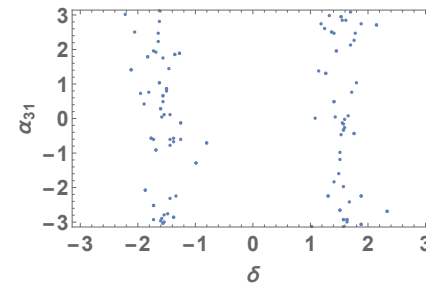


Figure 65: δ vs α_{31} (I)-C in IH

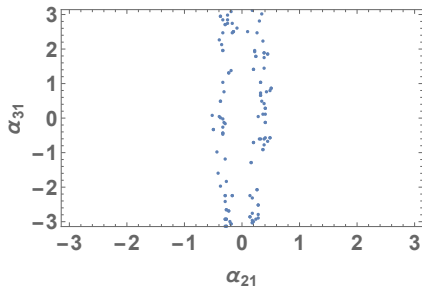


Figure 66: α_{21} vs α_{31} (I)-C in IH

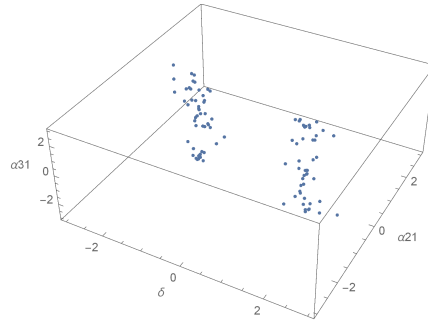


Figure 67: δ vs α_{21} vs α_{31} (I)-C in IH

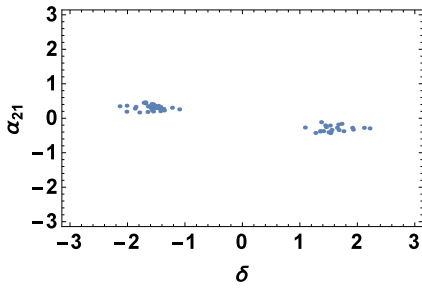


Figure 68: δ vs α_{21} (III)-A in IH

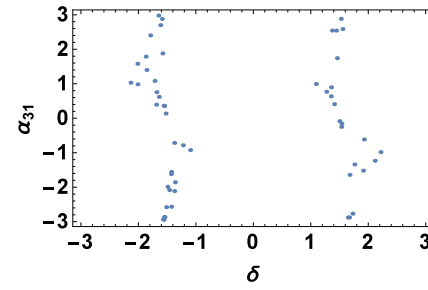


Figure 69: δ vs α_{31} (III)-A in IH

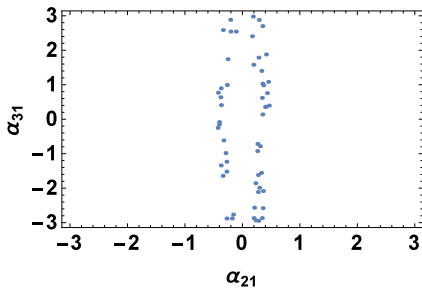


Figure 70: α_{21} vs α_{31} (III)-A in IH

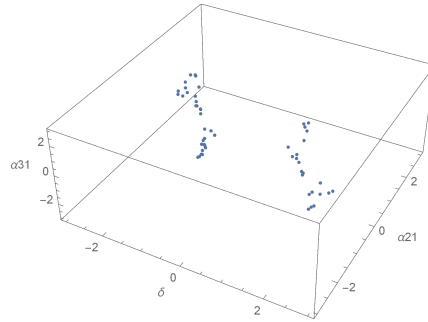


Figure 71: δ vs α_{21} vs α_{31} (III)-A in IH

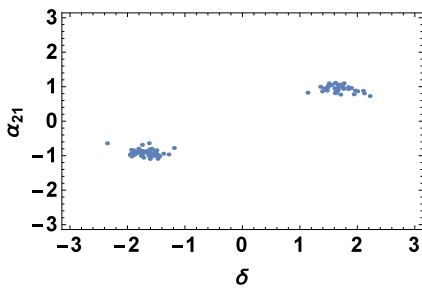


Figure 72: δ vs α_{21} (III)-B in IH

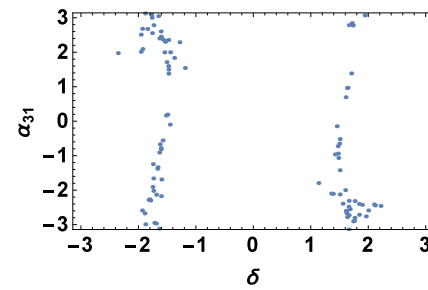


Figure 73: δ vs α_{31} (III)-B in IH

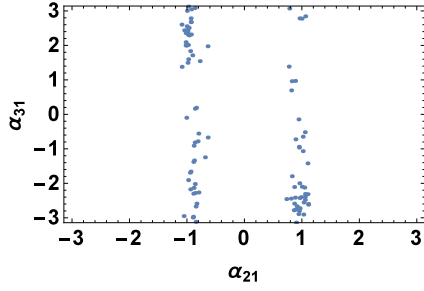


Figure 74: α_{21} vs α_{31} (III)-B in IH

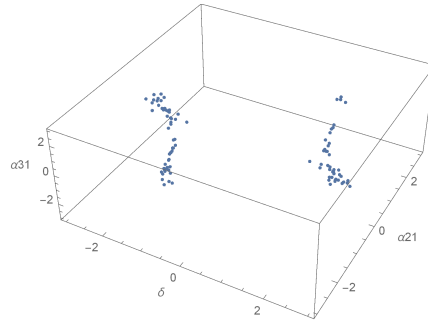


Figure 75: δ vs α_{21} vs α_{31} (III)-B in IH

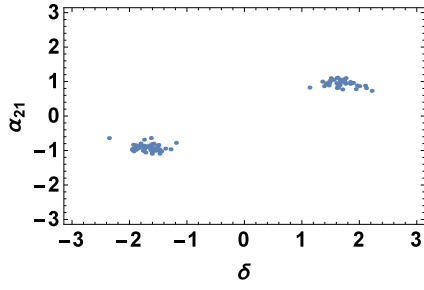


Figure 76: δ vs α_{21} (III)-E in IH

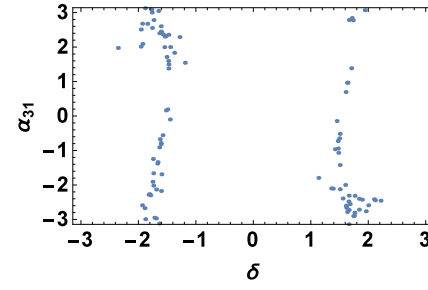


Figure 77: δ vs α_{31} (III)-E in IH

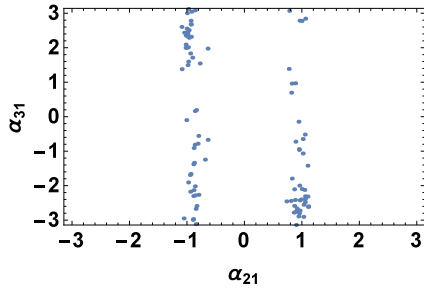


Figure 78: α_{21} vs α_{31} (III)-E in IH

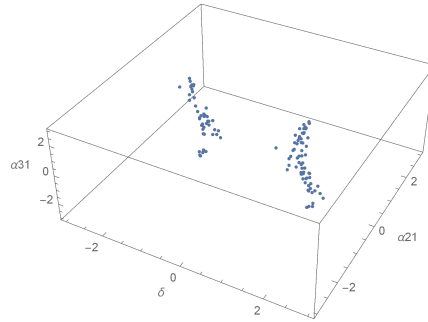


Figure 79: δ vs α_{21} vs α_{31} (III)-E in IH

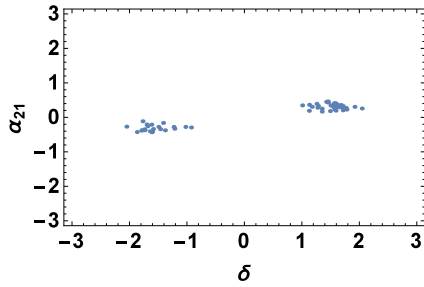


Figure 80: δ vs α_{21} (III)-F in IH

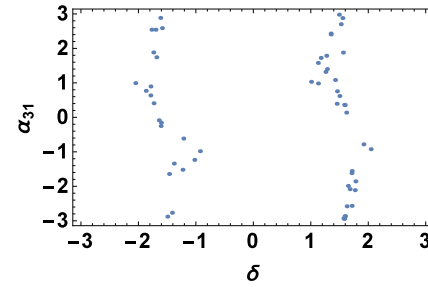


Figure 81: δ vs α_{31} (III)-F in IH

zero-elements-configuration on m_{eff} . Three of them correspond to the zero-off-diagonal elements of m_{eff} . The other case corresponds to the m_{eff} whose all elements are non-zero.

$$(m_{eff})_{e\mu} = (m_{eff})_{\mu e} = 0, \quad (75)$$

$$(m_{eff})_{e\tau} = (m_{eff})_{\tau e} = 0, \quad (76)$$

$$(m_{eff})_{\mu\tau} = (m_{eff})_{\tau\mu} = 0, \quad (77)$$

$$(m_{eff})_{\alpha\beta} \neq 0 \quad (\alpha, \beta = e, \mu, \tau). \quad (78)$$

Regarding our four-zero textures on Dirac mass matrix, the textures in class (I) and class (III) automatically produce zero-elements on m_{eff} , while the textures in class (II) lead to a m_{eff} whose all elements are non-zero. We summarize it on the table below, which subclass of textures produces zeros on which elements of m_{eff} . The textures without zero-elements in m_{eff} are also shown in Table5.

Table 5: The textures on the effective mass matrix

	$(m_{\text{eff}})_{e\mu} = 0$	$(m_{\text{eff}})_{e\tau} = 0$	$(m_{\text{eff}})_{\mu\tau} = 0$	all elements are non-zero
m_{eff}	$\begin{pmatrix} * & 0 & * \\ 0 & * & * \\ * & * & * \end{pmatrix}$	$\begin{pmatrix} * & * & 0 \\ * & * & * \\ 0 & * & * \end{pmatrix}$	$\begin{pmatrix} * & * & * \\ * & * & 0 \\ * & 0 & * \end{pmatrix}$	$\begin{pmatrix} * & * & * \\ * & * & * \\ * & * & * \end{pmatrix}$
textures	(I)-C (III)-B (III)-E	(I)-B (III)-A (III)-F	(I)-A (III)-C (III)-D	(II)-A (II)-B (II)-C

Which off-diagonal element of m_{eff} is zero, determine the constraint among mass eigenvalues, mixing angles and CP phases. Describing each off-diagonal elements of m_{eff} in terms of $m_1, m_2, m_3, \theta_{12}, \theta_{13}, \theta_{23}, \delta, \alpha_{21}$, and α_{31} ,

$$(m_{\text{eff}})_{e\mu} = \frac{1}{2}(-m_1 c_{12}^2 e^{i\delta} - m_2 s_{12}^2 e^{i(\alpha_{21} + \delta)} + m_3 e^{i(\alpha_{31} - \delta)}) s_{23} \sin 2\theta_{13} + \frac{1}{2}(-m_1 + m_2 e^{i\alpha_{21}}) c_{13} c_{23} \sin 2\theta_{12}, \quad (79)$$

$$(m_{\text{eff}})_{e\tau} = \frac{1}{2}(-m_1 c_{12}^2 e^{i\delta} - m_2 s_{12}^2 e^{i(\alpha_{21} + \delta)} + m_3 e^{i(\alpha_{31} - \delta)}) c_{23} \sin 2\theta_{13} + \frac{1}{2}(m_1 - m_2 e^{i\alpha_{21}}) c_{13} s_{23} \sin 2\theta_{12}, \quad (80)$$

$$(m_{\text{eff}})_{\mu\tau} = \frac{1}{2}\{m_1(c_{12}^2 s_{13}^2 e^{2i\delta} - s_{12}^2) + m_2(s_{12}^2 s_{13}^2 e^{i(\alpha_{21} + 2\delta)} - c_{12}^2 e^{i\alpha_{21}}) + m_3 c_{13}^2 e^{i\alpha_{31}}\} \sin 2\theta_{23} + \frac{1}{2}(m_1 e^{i\delta} - m_2 e^{i(\alpha_{21} + \delta)}) s_{13} \cos 2\theta_{23} \sin 2\theta_{12}. \quad (81)$$

$$s_{ij} = \sin \theta_{ij}, c_{ij} = \cos \theta_{ij} \quad (i, j = 1, 2, 3)$$

If an element $(m_{\text{eff}})_{e\mu}$ is equal to 0, both $\text{Re}(m_{\text{eff}})_{e\mu}$ and $\text{Im}(m_{\text{eff}})_{e\mu}$ must be 0. Let us then define functions f_1 and f_2 of three mass eigenvalues, three CP phases, and mixing angles,

$$f_1 = -\frac{m_1 c_{12}^2 \cos \delta + m_2 s_{12}^2 \cos(\alpha_{21} + \delta) - m_3 \cos(\alpha_{31} - \delta)}{m_1 - m_2 \cos \alpha_{21}}, \quad (82)$$

$$f_2 = \frac{m_1 c_{12}^2 \sin \delta + m_2 s_{12}^2 \sin(\alpha_{21} + \delta) - m_3 \sin(\alpha_{31} - \delta)}{m_2 \sin \alpha_{21}}, \quad (83)$$

and a function of mixing angles,

$$Y_1 = \frac{\sin 2\theta_{12}}{2 \sin \theta_{13} \tan \theta_{23}}. \quad (84)$$

The condition that $(m_{\text{eff}})_{e\mu} = 0$ is identical to that

$$f_1 = Y_1, \quad (85)$$

$$f_2 = Y_1. \quad (86)$$

After substituting the experimental values of mixing angles and mass squared differences Δm_{sol}^2 and Δm_{atm}^2 , f_1 and f_2 are regarded as functions of the lightest neutrino mass and three CP phases, while the value of Y_1 is determined. Eq.(85) and Eq.(86) imply that there are two conditions for four variables m_1 (m_3), δ , α_{21} , and α_{31} .

As for the condition that $(m_{\text{eff}})_{e\tau} = 0$, defining a function Y_2 of mixing angles

$$Y_2 = -\frac{\sin 2\theta_{12} \tan \theta_{23}}{2 \sin \theta_{13}}, \quad (87)$$

two conditions among the lightest neutrino mass and CP phases are written as

$$f_1 = Y_2, \quad (88)$$

$$f_2 = Y_2. \quad (89)$$

We note that the same functions f_1 and f_2 defined in Eq.(82) and in Eq.(83) appear in Eq.(88) and Eq.(89).

As for the condition that $(m_{\text{eff}})_{\mu\tau} = 0$, it is written as

$$f_3 = Y_3, \quad (90)$$

$$f_4 = Y_3. \quad (91)$$

where

$$f_3 = \frac{m_1(c_{12}^2 s_{13}^2 \cos 2\delta - s_{13}^2) + m_2(s_{12}^2 s_{13}^2 \cos(\alpha_{21} + 2\delta) - c_{12}^2 \cos \alpha_{21}) + m_3 c_{13}^2 \cos \alpha_{31}}{m_1 \cos \delta - m_2 \cos(\alpha_{21} + \delta)}, \quad (92)$$

$$f_4 = \frac{m_1 c_{12}^2 s_{13}^2 \sin 2\delta + m_2(s_{12}^2 s_{13}^2 \sin(\alpha_{21} + 2\delta) - c_{12}^2 \sin \alpha_{21}) + m_3 c_{13}^2 \sin \alpha_{31}}{m_1 \sin \delta - m_2 \sin(\alpha_{21} + \delta)}, \quad (93)$$

and

$$Y_3 = -\frac{\sin 2\theta_{12} \sin \theta_{13}}{\tan 2\theta_{23}}. \quad (94)$$

Also in the case of m_{eff} whose all elements are not zero, we can find conditions among the lightest neutrino mass and three CP phases. Such m_{eff} is made of a Dirac mass matrix with textures in class(II). By taking an example from the subclass(II)-B, a Dirac mass matrix of the texture

$$\begin{pmatrix} \sin \theta_1 \cos \theta_2 & 0 & 0 \\ \sin \theta_1 \sin \theta_2 & e^{i\phi_1} & 0 \\ \cos \theta_1 & 0 & e^{i\phi_2} \end{pmatrix} \quad (95)$$

produces the effective mass matrix

$$m_{eff} = - \begin{pmatrix} X_1 \sin^2 \theta_1 \cos^2 \theta_2 & \frac{1}{2} X_1 \sin^2 \theta_1 \sin 2\theta_2 & \frac{1}{2} X_1 \sin 2\theta_1 \cos \theta_2 \\ \frac{1}{2} X_1 \sin^2 \theta_1 \sin 2\theta_2 & X_1 \sin^2 \theta_1 \sin^2 \theta_2 + X_2 e^{2i\phi_1} & \frac{1}{2} X_1 \sin 2\theta_1 \sin \theta_2 \\ \frac{1}{2} X_1 \sin 2\theta_1 \cos \theta_2 & \frac{1}{2} X_1 \sin 2\theta_1 \sin \theta_2 & X_3 e^{2i\phi_2} \end{pmatrix}. \quad (96)$$

Let us consider a quantity independent of the phase redefinition for charged lepton's flavor basis,

$$\frac{(m_{eff})_{ee}(m_{eff})_{\mu\tau}}{(m_{eff})_{e\mu}(m_{eff})_{e\tau}}. \quad (97)$$

If m_{eff} is given as Eq.(96), the product equals to 1.

$$\frac{(m_{eff})_{ee}(m_{eff})_{\mu\tau}}{(m_{eff})_{e\mu}(m_{eff})_{e\tau}} = 1 \quad (98)$$

We generalize this condition to the all textures in class(II). Setting α as the row component which has only one non-zero elements on the Dirac mass matrix in a texture of class(II), and β and γ as the other row components which have two non-zero elements, the generalization of Eq.(98) is

$$\frac{(m_{eff})_{\alpha\alpha}(m_{eff})_{\beta\gamma}}{(m_{eff})_{\alpha\beta}(m_{eff})_{\alpha\gamma}} = 1. \quad (99)$$

$$(\alpha, \beta, \gamma = e, \mu, \tau \quad \alpha \neq \beta \neq \gamma)$$

Eq.(99) is symmetric with respect to the exchange between β and γ . For the case of the subclass (II)-A, α stands for τ . For the subclass (II)-B and (II)-C, α stands for e and μ respectively. Rewriting the elements of m_{eff} in terms of mass eigenvalues, mixing angles, and CP phases, we obtain two conditions among them.

$$\text{Re}\left(\frac{(m_{eff})_{\alpha\alpha}(m_{eff})_{\beta\gamma}}{(m_{eff})_{\alpha\beta}(m_{eff})_{\alpha\gamma}}\right) = 1 \quad (100)$$

$$\text{Im}\left(\frac{(m_{eff})_{\alpha\alpha}(m_{eff})_{\beta\gamma}}{(m_{eff})_{\alpha\beta}(m_{eff})_{\alpha\gamma}}\right) = 0 \quad (101)$$

Eq.(99) is also rewritten as

$$\text{Re}\{(m_{eff})_{\alpha\alpha}(m_{eff})_{\beta\gamma}\} = \text{Re}\{(m_{eff})_{\alpha\beta}(m_{eff})_{\alpha\gamma}\}, \quad (102)$$

$$\text{Im}\{(m_{eff})_{\alpha\alpha}(m_{eff})_{\beta\gamma}\} = \text{Im}\{(m_{eff})_{\alpha\beta}(m_{eff})_{\alpha\gamma}\}. \quad (103)$$

Each condition, Eq.(102) or Eq.(103), is dependent on phase redefinition. However, two conditions all together are equivalent to Eq.(99).

6.2 Explanations for the results of numerical analysis

In this subsection, we give detailed explanations for the correlations among CP phases in section 5.3.3 from a view point of the conditions discussed in Sec.6.1. The constraints obtained in Sec.6.1 describe the relations as for CP phases δ , α_{21} and α_{31} . We first show the relations among CP phases from $(m_{eff})_{e\mu} = 0$ in IH case and from $(m_{eff})_{e\tau} = 0$ in IH case, in Figs.(84)-(89), which lead to a good explanation for the scatter plots in section 5.3.3 of the corresponding four-zero texture. $(m_{eff})_{\mu\tau} = 0$ in NH case and the subclass (II)-B in IH case do not have allowed region under the constraints. It is shown in Figs.(90)-(95). These two unfavorable cases correspond to the four-zero textures which produce no scatter plots in section 5. We also mention the constraints from $(m_{eff})_{e\tau} = 0$ in NH case. Although it seems that there is less obvious relation between them in comparison with the former cases, it is not inconsistent with the results of scatter plots. We show the obtained relations in Figs.(96)-(98) and clarify the reason.

6.2.1 $(m_{eff})_{e\mu} = 0$ in IH case

We first investigate the textures of subclasses (I)-C, (III)-B and (III)-E, which produce 0 on $(m_{eff})_{e\mu}$, in inverted hierarchical case. The results of numerical analysis for these textures in IH case are shown in Fig.(64), Fig.(72), Fig.(80), Fig.(65), Fig.(73) and Fig.(81). Let us compare these plotted points on the two-dimensional planes (δ, α_{21}) and (δ, α_{31}) with constraints among δ , α_{21} and α_{31} under the condition Eq.(85) and Eq.(86). In IH case, two mass eigenvalues m_1 and m_2 are written as the functions of the lightest neutrino mass m_3 by using experimental values of the mass squared differences Δm_{sol}^2 and Δm_{atm}^2 . After substituting the values of three mixing angles and determining the value of m_3 , f_1 and f_2 are functions of three CP phases, and Y_1 has a unique value. Eq.(85) and Eq.(86) imply two independent conditions for three CP phases δ , α_{21} and α_{31} .

For some given values of m_3 , we draw two curved surfaces which are described by Eq.(85) and Eq.(86) on a 3-dimensional space spanned by δ , α_{21} and α_{31} . We substitute values of m_3 by dividing it into several intervals from 0 eV to its upper bound 0.046 eV. The points on the nodal line of two curved surfaces indicate the possible ranges of CP phases under the condition of the vanishing element $(m_{eff})_{e\mu} = 0$. We show three examples of such 3-dimensional plots on $(\delta, \alpha_{21}, \alpha_{31})$ space, by taking m_3 as 0 eV, the half-value of its upper bound 0.023 eV and its upper bound 0.046 eV.

The yellow and blue curved surfaces in Figs.(84)-(86) are described by Eq.(85) and Eq.(86) respectively. Two surfaces vary smoothly depending on the value of the lightest neutrino mass m_3 . Focusing on (δ, α_{21}) planes, it can be seen that the features which we have discussed in Fig.(64), Fig.(72) and Fig.(80) are reflected in Figs.(84)-(86). By contrast, they show that α_{31} ranges from $-\pi$ to π without strong dependence on δ nor α_{21} . This result corresponds to Fig.(65), Fig.(73) and Fig.(81).

6.2.2 $(m_{eff})_{e\tau} = 0$ in IH case

We apply the discussion in Sec.6.2.1 to another element $(m_{eff})_{e\tau}$ of the effective mass matrix. The results of numerical analysis for textures (I)-B, (III)-A and

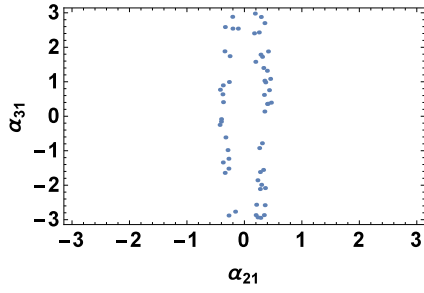


Figure 82: α_{21} vs α_{31} (III)-F in IH

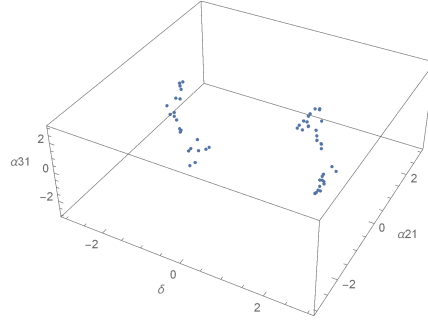


Figure 83: δ vs α_{21} vs α_{31} (III)-F in IH

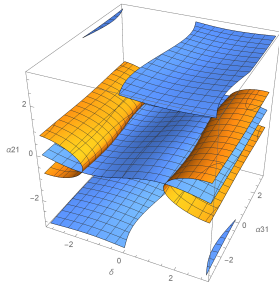


Figure 84: Contour plots on $(\delta, \alpha_{21}, \alpha_{31})$ under the condition $(m_{\text{eff}})_{e\mu} = 0$ in IH, where $m_3=0$ eV

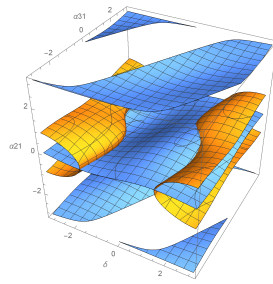


Figure 85: Contour plots on $(\delta, \alpha_{21}, \alpha_{31})$ under the condition $(m_{\text{eff}})_{e\mu} = 0$ in IH, where $m_3=0.023$ [eV]

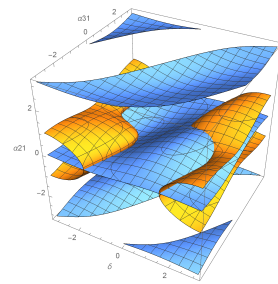


Figure 86: Contour plots on $(\delta, \alpha_{21}, \alpha_{31})$ under the condition $(m_{\text{eff}})_{e\mu} = 0$ in IH, where $m_3=0.046$ eV

(III)-F are shown in Fig.(60), Fig.(68), Fig.(76), Fig.(61), Fig.(69) and Fig.(77). These textures produce that $(m_{\text{eff}})_{e\tau}$ equals 0. In this case, three CP phases and the lightest neutrino mass follow the conditions Eq.(88) and Eq.(89). By imposing the IH case and using the experimental values, we obtain two constraints for three CP phases. Drawing two curved surfaces described by Eq.(88) and Eq.(89) on $(\delta, \alpha_{21}, \alpha_{31})$ space for several values of m_3 , we find nodal lines of them. We show three examples in the cases of 0, the half-value of the upper bound and the upper bound of m_3 . The yellow and blue curved surfaces in Figs.(87)-(89) stand for Eq.(88) and Eq.(89) respectively. The allowed values on $(\delta, \alpha_{21}, \alpha_{31})$ space from two curved surfaces show the similar features as Figs.(84)-(86).

6.2.3 $(m_{\text{eff}})_{\mu\tau} = 0$ in NH case

We have mentioned that subclasses (I)-A, (III)-C and (III)-D, which produce 0 on $(m_{\text{eff}})_{\mu\tau}$, were not consistent with the experimental data in normal hierarchy case. It can be explained by the conditions Eq.(90) and Eq.(91). In NH case, two mass eigenvalues m_2 and m_3 are written as the functions of the lightest neutrino mass m_1 . By using the experimental values of mixing angles and determining the value of m_1 , Eq.(90) and Eq.(91) can be regarded as two independent conditions for three CP phases. We can draw them on $(\delta, \alpha_{21}, \alpha_{31})$ space. The value of m_1 is taken similarly by several intervals from 0 eV to 0.046 eV. Two curved surfaces vary smoothly depending on m_1 . As the value of m_1 is increased, these surfaces are approaching to each other. However, they do not intersect within the upper limit of m_1 . We show three examples for $m_1 = 0, 0.023$ and 0.046 eV. The yellow and blue curved surfaces in Figs.(90)-(92) stand for Eq.(90) and Eq.(91) respectively. Therefore, the textures whose $(m_{\text{eff}})_{\mu\tau}$ is equal to zero do not reproduce the experimentally measured mixing angles and mass eigenvalues in NH case.

6.2.4 subclass (II)-B in IH case

let us explain the other case which do not lead to the experimental data, the subclass (II)-B in IH case. The constraints among CP phases for the (II)-B are Eq.(102) and Eq.(103) by setting α as e . The yellow and blue curved surfaces in Fig.(93) to (95) stand for Eq.(102) and Eq.(103) respectively. Although two curved surfaces vary smoothly depending on the lightest neutrino mass m_3 from 0 eV to 0.046 eV, they never intersect for any intervals of m_3 . It implies that the texture of (II)-B do not reproduce the experimentally measured mixing angles and mass eigenvalues in IH case.

6.2.5 $(m_{\text{eff}})_{e\tau} = 0$ in NH case

We also mention the result in Fig.(48) with constraints among δ, α_{21} and α_{31} under the condition Eq.(88) and Eq.(89). In this case, there is no inconsistency between scatter plots from four-zero texture and 3D plots from one-zero effective light neutrino mass matrix. However, we do not find obvious relation between them in comparison with the former cases. The yellow and blue curved surfaces in Figs.(96)-(98) are described by Eq.(88) and Eq.(89) respectively. The correspondence between Fig.(48) and contour plots can be seen in a range of large m_1 .

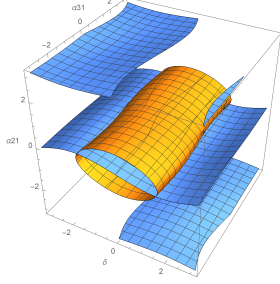


Figure 87: Contour plots on $(\delta, \alpha_{21}, \alpha_{31})$ under the condition $(m_{\text{eff}})_{e\tau} = 0$ in IH, where $m_3=0$ eV

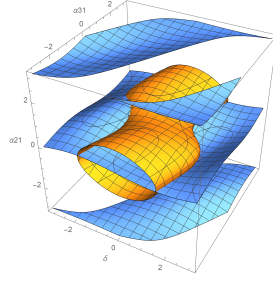


Figure 88: Contour plots on $(\delta, \alpha_{21}, \alpha_{31})$ under the condition $(m_{\text{eff}})_{e\tau} = 0$ in IH, where $m_3=0.023$ eV

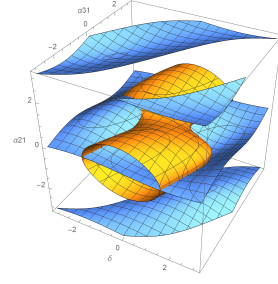


Figure 89: Contour plots on $(\delta, \alpha_{21}, \alpha_{31})$ under the condition $(m_{\text{eff}})_{e\tau} = 0$ in IH, where $m_3=0.046$ eV

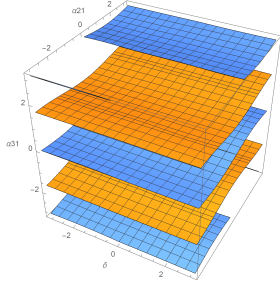


Figure 90: Contour plots on $(\delta, \alpha_{21}, \alpha_{31})$ under the condition $(m_{\text{eff}})_{\mu\tau} = 0$ in NH, where $m_1=0$ eV

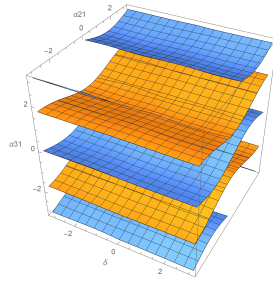


Figure 91: Contour plots on $(\delta, \alpha_{21}, \alpha_{31})$ under the condition $(m_{\text{eff}})_{\mu\tau} = 0$ in NH, where $m_1=0.023$ eV

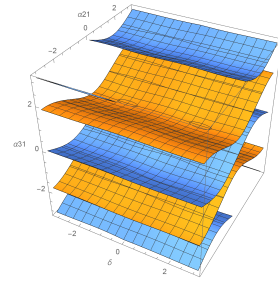


Figure 92: Contour plots on $(\delta, \alpha_{21}, \alpha_{31})$ under the condition $(m_{\text{eff}})_{\mu\tau} = 0$ in NH, where $m_1=0.046$ eV

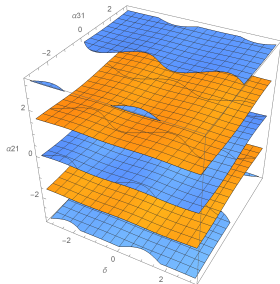


Figure 93: Contour plots on $(\delta, \alpha_{21}, \alpha_{31})$ for subclass (II)-B in IH, where $m_3=0$ eV

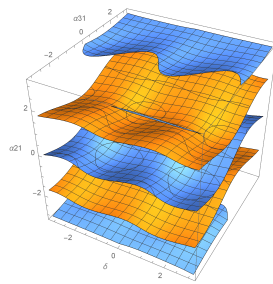


Figure 94: Contour plots on $(\delta, \alpha_{21}, \alpha_{31})$ for subclass (II)-B in IH, where $m_3=0.023$ eV

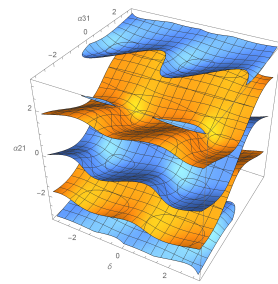


Figure 95: Contour plots on $(\delta, \alpha_{21}, \alpha_{31})$ for subclass (II)-B in IH, where $m_3=0.046$ eV

From the viewpoint of (δ, α_{21}) planes of Fig.(97) and Fig.(98), the nodal lines of two surfaces do not completely overlap the range of plotted points in Fig.(48). The reasons are as follows: The four-zero texture in Fig.(48) is one part of the textures which produce $(m_{eff})_{e\tau} = 0$. There is no one-to-one correspondence between the results from Fig.(48) in numerical analysis and from Figs.(96)-(98). Besides, only the central values of mixing angles and mass squared differences are chosen to draw the 3-dimensional plots, while these values in the scattered plots are taken within 3 standard deviations from the mean of the experimental values.

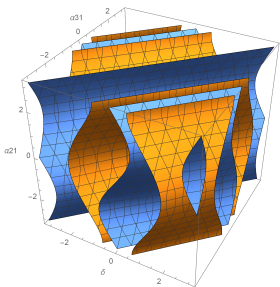


Figure 96: Contour plots on $(\delta, \alpha_{21}, \alpha_{31})$ under the condition $(m_{eff})_{e\tau} = 0$ in NH, where $m_1=0$ eV

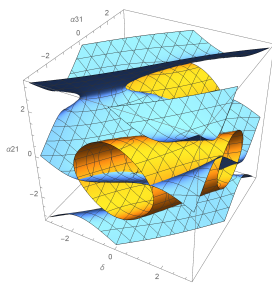


Figure 97: Contour plots on $(\delta, \alpha_{21}, \alpha_{31})$ under the condition $(m_{eff})_{e\tau} = 0$ in NH, where $m_1=0.023$ [eV]

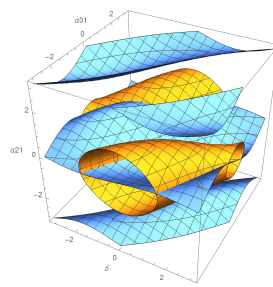


Figure 98: Contour plots on $(\delta, \alpha_{21}, \alpha_{31})$ under the condition $(m_{eff})_{e\tau} = 0$ in NH, where $m_1=0.046$ eV

7 Discussions and Summary

We have introduced the type-(I) seesaw mechanism as an attractive extension for the Standard Model to explain the mass of neutrinos. The effective mass matrix for left-handed Majorana neutrinos m_{eff} is expressed with nine phenomenological parameters: two mass squared differences, the lightest neutrino mass, one Dirac and two Majorana CP phases. In this paper, we have investigated the four-zero texture model for the Dirac mass matrix. We have classified ${}_9C_4 = 126$ different textures for Dirac neutrino mass matrix into seven classes according to the configurations of zero or non-zero elements. This classification allows us to distinguish which texture produces three massive neutrino eigenvalues and which texture leads to a non-zero Jarlskog invariant. We have investigated three classes (I), (II) and (III) which are able to explain the three non-zero masses and CP violation in the neutrino sector. m_{eff} s in these classes include seven model parameters $(\theta_1, \theta_2, \phi_1, \phi_2, X_1, X_2, \text{ and } X_3)$.

We have outlined how to make numerical analysis for our model. The procedure of calculation can be efficiently done by defining the sub-classification. Each sub-class consists of six textures which construct the same effective neutrino mass matrix neutrinos m_{eff} , so that these six textures are regarded as the same model to study the mass eigenvalues, the mixing angles and the CP phases. We have taken the model parameters which reproduce two mass squared differences and three mixing angles within 3 standard deviations from the mean

of experimental values. Since the number of model parameters is reduced to seven, the correlation among CP violating phases can be predictions after assuming the neutrino mass hierarchy and after substituting an allocated value of the lightest neutrino mass. The correlations among model parameters, among mass eigenvalues and among CP phases are shown.

We have also made analysis from the view point of the effective Majorana neutrino mass matrix m_{eff} . Some textures of the Dirac mass matrix produce one zero-element on an off-diagonal part of the m_{eff} . One vanishing off-diagonal element on m_{eff} corresponds to two constraints. The other textures, which lead to nine non-vanishing elements of Majorana mass matrix, also produce two constraints because of the four-zero textures on the Dirac mass matrix. We found the hidden relations among CP violating phases after assuming the value of the lightest neutrino mass. These hidden relations correspond to the four-zero texture for the Dirac neutrino mass matrix. In particular, the subclasses which do not produce any scattered plots in numerical analysis are explained by means of 3D plot among CP violating phases. Such subclasses made no nodal lines of surfaces described by the conditions.

8 Appendix

8.1 The general Δ with full elements of the Dirac mass matrix

We show the form of Δ for the general Dirac mass matrix

$$\mathcal{U} = \begin{pmatrix} u_{e1} & u_{e2} & u_{e3} \\ u_{\mu1} & u_{\mu2} & u_{\mu3} \\ u_{\tau1} & u_{\tau2} & u_{\tau3} \end{pmatrix}. \quad (104)$$

The Δ is described by the definition in Eq.(28) in terms of \mathcal{U} in Eq.(104)

and X in Eq.(31).

$$\begin{aligned}
\Delta = & \sum_{\{\alpha,\beta,\gamma\}} \sum_{\{p,q,r\}} X_p^4 X_q^2 (1 - |A_{pq}|^2) |u_{\alpha p}|^2 \text{Im}(u_{\beta p}^* u_{\beta q} u_{\gamma q}^* u_{\gamma p}) \\
& + \sum_{\{\alpha,\beta,\gamma\}} \sum_{\{p,q,r\}} X_p^4 X_q X_r |u_{\alpha p}|^2 \text{Im}(A_{rq} u_{\beta p}^* u_{\beta q} u_{\tau r}^* u_{\gamma p} + A_{pq} A_{rp} u_{\beta r}^* u_{\beta p} u_{\gamma p}^* u_{\tau q}) \\
& + \sum_{\{\alpha,\beta,\gamma\}} \sum_{\{p,q,r\}} X_p^3 X_q^3 (1 - |A_{pq}|^2) |u_{\beta p}|^2 |u_{\tau q}|^2 \text{Im}(A_{qp} u_{\alpha q}^* u_{\alpha p}) \\
& + \sum_{\{\alpha,\beta,\gamma\}} X_1^2 X_2^2 X_3^2 \{ \text{Im}(u_{\alpha 1}^* u_{\alpha 2} u_{\beta 1}^* u_{\beta 3} u_{\gamma 3}^* u_{\gamma 1}) \\
& \quad + \text{Im}(A_{21} A_{13} A_{32} u_{\alpha 1}^* u_{\alpha 2} u_{\beta 3}^* u_{\beta 1} u_{\gamma 2}^* u_{\gamma 3}) \\
& \quad + |u_{\alpha 1}|^2 |u_{\beta 1}|^2 |u_{\tau 2}|^2 \text{Im}(A_{12} A_{32} A_{13}) \} \} \\
& + \sum_{\{\alpha,\beta,\gamma\}} \sum_{\{p,q,r\}} X_1^2 X_2^2 X_3^2 \{ \text{Im}(A_{pq} A_{rq} A_{pr} u_{\alpha p}^* u_{\alpha q} u_{\beta r}^* u_{\beta q} u_{\gamma p}^* u_{\gamma r}) \\
& \quad + |A_{pq}|^2 |u_{\alpha p}|^2 \text{Im}(u_{\beta q}^* u_{\beta r} u_{\gamma r}^* u_{\gamma q}) + \text{Im}(A_{pq}^2 u_{\alpha q}^* u_{\alpha r} u_{\beta p}^* u_{\beta r} u_{\gamma p}^* u_{\gamma q}) \} \\
& + \sum_{\{\alpha,\beta,\gamma\}} \sum_{\{p,q,r\}} X_p^3 X_q^2 X_r \{ |u_{\alpha p}|^2 \text{Im}(A_{pq}^2 A_{rp} u_{\beta r}^* u_{\beta q} u_{\gamma p}^* u_{\tau q} + A_{qp}^2 A_{pr} u_{\beta q}^* u_{\beta p} u_{\tau q}^* u_{\tau r}) \\
& \quad + A_{pq} A_{rq} u_{\beta p}^* u_{\beta q} u_{\gamma r}^* u_{\gamma q} + A_{qp} A_{qr} u_{\beta q}^* u_{\beta r} u_{\gamma p}^* u_{\gamma p}) \\
& \quad + \text{Im}(A_{qp} A_{rq} u_{\alpha r}^* u_{\alpha p} (|u_{\beta p}|^2 |u_{\gamma q}|^2 + u_{\beta q}^* u_{\beta p} u_{\gamma p}^* u_{\gamma q})) \\
& \quad + A_{pq} A_{qr} u_{\alpha p}^* u_{\alpha r} (|u_{\beta q}|^2 |u_{\gamma p}|^2 + u_{\beta q}^* u_{\beta p} u_{\gamma p}^* u_{\gamma q}) \\
& \quad + A_{rp} u_{\alpha q}^* u_{\alpha p} (|u_{\beta p}|^2 u_{\gamma r}^* u_{\gamma q} + u_{\beta r}^* u_{\beta p} u_{\gamma p}^* u_{\gamma q}) \\
& \quad + A_{rp} |A_{pq}|^2 |u_{\alpha p}|^2 (u_{\beta q}^* u_{\beta p} u_{\gamma r}^* u_{\gamma q} + u_{\beta r}^* u_{\beta p} |u_{\gamma q}|^2) \\
& \quad + A_{pr} |A_{pq}|^2 |u_{\alpha p}|^2 (u_{\beta q}^* u_{\beta r} u_{\gamma p}^* u_{\gamma q} + |u_{\beta q}|^2 u_{\gamma p}^* u_{\gamma q}) \},
\end{aligned} \tag{105}$$

where α, β, γ denote the different flavors,

$$\alpha, \beta, \gamma = e, \mu, \tau \quad (\alpha \neq \beta \neq \gamma). \tag{106}$$

p, q, r denote the different numbers 1, 2 or 3,

$$p, q, r = 1, 2, 3 \quad (p \neq q \neq r). \tag{107}$$

We define the sums $\sum_{\{\alpha,\beta,\gamma\}}$ and $\sum_{\{p,q,r\}}$ such that they take all possible combinations of indexes (α, β, γ) and (p, q, r) . For example,

$$\sum_{\{\alpha,\beta,\gamma\}} |u_{\alpha 1}|^2 = |u_{e1}|^2 + |u_{\mu 1}|^2 + |u_{\tau 1}|^2 \tag{108}$$

$$\begin{aligned}
\sum_{\{\alpha,\beta,\gamma\}} u_{\alpha 1} u_{\beta 2}^* = & u_{e1} u_{\mu 2}^* + u_{\mu 1} u_{e2}^* + u_{e1} u_{\tau 2}^* \\
& + u_{\tau 1} u_{e2}^* + u_{\mu 1} u_{\tau 2}^* + u_{\tau 1} u_{\mu 2}^*
\end{aligned} \tag{109}$$

If we take $X_3 = 0$, the discussion turns to the model with only two heavy right-handed neutrinos. As a consequence, this model leads to that one of the

lite neutrino mass eigenvalues corresponds to zero. The m_{eff} of such model expressed in terms of six components of a three by two Dirac mass matrix and two X_1, X_2 .

$$m_{eff} = - \begin{pmatrix} u_{e1} & u_{e2} \\ u_{\mu 1} & u_{\mu 2} \\ u_{\tau 1} & u_{\tau 2} \end{pmatrix} \begin{pmatrix} X_1 & 0 \\ 0 & X_2 \end{pmatrix} \begin{pmatrix} u_{e1} & u_{\mu 1} & u_{\tau 1} \\ u_{e2} & u_{\mu 2} & u_{\tau 2} \end{pmatrix} \quad (110)$$

Δ is

$$\begin{aligned} \Delta = \sum_{\{\alpha, \beta, \gamma\}} & \{X_1^4 X_2^2 (1 - |A_{12}|^2) |u_{\alpha 1}|^2 \text{Im}(u_{\beta 1}^* u_{\beta 2} u_{\gamma 2}^* u_{\gamma 1}) \\ & + X_2^4 X_1^2 (1 - |A_{12}|^2) |u_{\alpha 2}|^2 \text{Im}(u_{\beta 2}^* u_{\beta 1} u_{\gamma 1}^* u_{\gamma 2}) \\ & + X_1^3 X_2^3 (1 - |A_{12}|^2) |u_{\beta 1}|^2 |u_{\gamma 2}|^2 \text{Im}(A_{21} u_{\alpha 2}^* u_{\alpha 1})\}. \end{aligned} \quad (111)$$

8.2 The m_{eff} and Δ with concrete parametrization for each class

In section 4, we have classified all four-zero textures into seven classes and illustrate one representation of texture for each class in Eq.57-Eq.57. We quote these seven representation with concrete parametrization again and also show the accompanying m_{eff} and Δ derived from each concrete texture.

(I) There is only one row component in which all elements are non-zero, and rank $\mathcal{U} = 3$.

$$\mathcal{U}^{(I)} = \begin{pmatrix} c_1 e^{i\phi_1} & c_2 e^{i\phi_2} & 1 \\ s_1 & 0 & 0 \\ 0 & s_2 & 0 \end{pmatrix} \quad (112)$$

The effective mass matrix is

$$m_{eff}^{(I)} = - \begin{pmatrix} X_1 c_1^2 e^{2i\phi_1} + X_2 c_2^2 e^{2i\phi_2} + X_3 & \frac{1}{2} X_1 \sin 2\theta_1 e^{i\phi_1} & \frac{1}{2} X_2 \sin 2\theta_2 e^{i\phi_2} \\ \frac{1}{2} X_1 \sin 2\theta_1 e^{i\phi_1} & X_1 s_1^2 & 0 \\ \frac{1}{2} X_2 \sin 2\theta_2 e^{i\phi_2} & 0 & X_2 s_2^2 \end{pmatrix} \quad (113)$$

$$\begin{aligned} \Delta^{(I)} = \frac{1}{4} X_1^2 X_2^2 s_1^2 \sin^2 2\theta_2 \{ & X_1 X_2 (1 - c_1^2 c_2^2) c_1^2 \sin 2(\phi_1 - \phi_2) \\ & + (X_1 + X_3) X_3 c_1^2 \sin 2\phi_1 - X_2 X_3 \sin 2\phi_2 \} \end{aligned} \quad (114)$$

(II) There is only one column component in which all elements are non-zero, and rank $\mathcal{U} = 3$.

$$\mathcal{U}^{(II)} = \begin{pmatrix} s_1 c_2 & e^{i\phi_1} & 0 \\ s_1 s_2 & 0 & e^{i\phi_2} \\ c_1 & 0 & 0 \end{pmatrix} \quad (115)$$

The effective mass matrix is

$$m_{eff}^{(II)} = - \begin{pmatrix} X_1 s_1^2 c_2^2 + X_2 e^{2i\phi_1} & \frac{1}{2} X_1 s_1^2 \sin 2\theta_2 & \frac{1}{2} X_1 \sin 2\theta_1 c_2 \\ \frac{1}{2} X_1 s_1^2 \sin 2\theta_2 & X_1 s_1^2 s_2^2 + X_3 e^{2i\phi_2} & \frac{1}{2} X_1 \sin 2\theta_1 s_2 \\ \frac{1}{2} X_1 \sin 2\theta_1 c_2 & \frac{1}{2} X_1 \sin 2\theta_1 s_2 & X_1 c_1^2 \end{pmatrix} \quad (116)$$

$$\begin{aligned}
\Delta^{(\text{II})} = & \frac{1}{8} X_1^3 s_1^2 c_2 \sin^2 2\theta_1 \sin 2\theta_2 \{ X_1^2 X_2 (c_1 + s_1 - \frac{1}{2} c_1 s_2^2 \sin 2\theta_1) (c_1 - s_1 + \frac{1}{2} s_1 s_2 \sin 2\theta_2 \sin 2\phi_1) \\
& + X_1^2 X_3 s_2 (c_1 + \frac{1}{2} s_1 s_2 \sin 2\theta_2 (1 + c_1 + s_1 - \frac{1}{2} c_1 s_2^2 \sin 2\theta_1)) \sin 2\phi_2 \\
& + X_2^2 X_3 \sin 2\phi_2 + X_2 X_3^2 s_2 \sin 2\phi_1 \\
& + X_1 X_2 X_3 (-s_2 \sin 2(\phi_1 - \phi_2)) \\
& + (c_1 + c_1 s_2 + s_1 s_2 + s_1^2 c_2^2 + \frac{1}{2} s_1 s_2 \sin 2\theta_2 - \frac{1}{2} c_1 s_2^3 \sin 2\theta_1) \sin 2(\phi_1 + \phi_2) \} \\
& \quad (117)
\end{aligned}$$

(III) There are one row and column components in which two elements are zero, and the common element on the both of such row and column is zero. Besides, we require that $\text{rank } \mathcal{U} = 3$.

$$\mathcal{U}^{(\text{III})} = \begin{pmatrix} c_1 & 0 & 0 \\ s_1 & c_2 e^{i\phi_1} & 0 \\ 0 & s_2 e^{i\phi_2} & 1 \end{pmatrix} \quad (118)$$

The effective mass matrix is

$$m_{eff}^{(\text{III})} = - \begin{pmatrix} X_1 c_1^2 & \frac{1}{2} X_1 \sin 2\theta_1 & 0 \\ \frac{1}{2} X_1 \sin 2\theta_1 & X_1 s_1^2 + X_2 c_2^2 e^{2i\phi_1} & \frac{1}{2} X_2 \sin 2\theta_2 e^{i(\phi_1 + \phi_2)} \\ 0 & \frac{1}{2} X_2 \sin 2\theta_2 e^{i(\phi_1 + \phi_2)} & X_2 s_2^2 e^{2i\phi_2} + X_2 \end{pmatrix} \quad (119)$$

$$\begin{aligned}
\Delta^{(\text{III})} = & \frac{1}{16} X_1^2 X_2^2 \sin^2 2\theta_1 \sin 2\theta_2 \{ X_1 X_2 (s_1 + s_2 - s_1^2 s_2^4) \sin 2\phi_1 \\
& + X_1 X_3 (s_1 + s_2) \sin 2(\phi_1 + \phi_2) + X_2 X_3 s_2^2 \sin 2\phi_2 \} \\
& \quad (120)
\end{aligned}$$

(IV) There is only one column component in which all elements are zero.

$$\mathcal{U}^{(\text{IV})} = \begin{pmatrix} s_1 c_2 & c_3 e^{i\phi_1} & 0 \\ s_1 s_2 & s_3 e^{i\phi_2} & 0 \\ c_1 & 0 & 0 \end{pmatrix} \quad (121)$$

The effective mass matrix is

$$m_{eff}^{(\text{IV})} = - \begin{pmatrix} X_1 s_1^2 c_2^2 + X_2 c_3^2 e^{2i\phi_1} & \frac{1}{2} (X_1 s_1^2 \sin 2\theta_2 + X_2 \sin 2\theta_3 e^{i(\phi_1 + \phi_2)}) & \frac{1}{2} X_1 \sin 2\theta_1 c_2 \\ \frac{1}{2} (X_1 s_1^2 \sin 2\theta_2 + X_2 \sin 2\theta_3 e^{i(\phi_1 + \phi_2)}) & X_1 s_1^2 s_2^2 + X_2 s_3^2 e^{2i\phi_2} & \frac{1}{2} X_1 \sin 2\theta_1 s_2 \\ \frac{1}{2} X_1 \sin 2\theta_1 c_2 & \frac{1}{2} X_1 \sin 2\theta_1 s_2 & X_1 c_1^2 \end{pmatrix} \quad (122)$$

$$\begin{aligned}
\Delta^{(\text{IV})} = & \frac{1}{16} X_1^3 X_2^2 \sin^2 2\theta_1 \sin 2\theta_2 \{ 1 - s_1^2 (c_2^2 c_3^3 + s_2^2 s_3^2) + \frac{1}{2} \sin 2\theta_2 \sin 2\theta_3 \cos(\phi_1 - \phi_2) \} \\
& \times \{ 2X_1 c_3 \sin(\phi_1 - \phi_2) + X_2 (c_2^2 \sin 2\theta_3 \sin 2\phi_1 - \sin 2\theta_2 \cos 2\theta_3 \sin(\phi_1 + \phi_2) - s_2^2 \sin 2\theta_3 \sin 2\phi_2) \} \\
& \quad (123)
\end{aligned}$$

(V) There is only one row component in which all elements are zero.

$$\mathcal{U}^{(V)} = \begin{pmatrix} c_1 & c_2 e^{i\phi_1} & e^{i\phi_3} \\ s_1 & s_2 e^{i\phi_2} & 0 \\ 0 & 0 & 0 \end{pmatrix} \quad (124)$$

The effective mass matrix is

$$m_{eff}^{(V)} = - \begin{pmatrix} X_1 c_1^2 + X_2 c_2^2 e^{2i\phi_1} + X_3 e^{2i\phi_3} & \frac{1}{2} X_1 \sin 2\theta_1 + \frac{1}{2} X_2 \sin 2\theta_2 e^{i(\phi_1+\phi_2)} & 0 \\ \frac{1}{2} X_1 \sin 2\theta_1 + \frac{1}{2} X_2 \sin 2\theta_2 e^{i(\phi_1+\phi_2)} & X_1 s_1^2 + X_2 s_2^2 e^{2i\phi_2} & 0 \\ 0 & 0 & 0 \end{pmatrix} \quad (125)$$

$$\Delta^{(V)} = 0 \quad (126)$$

(VI) There is one row component and one column component in which all elements are non-zero.

$$\mathcal{U}^{(VI)} = \begin{pmatrix} s_1 c_2 & e^{i\phi_1} & e^{i\phi_2} \\ s_1 s_2 & 0 & 0 \\ c_1 & 0 & 0 \end{pmatrix} \quad (127)$$

The effective mass matrix is

$$m_{eff}^{(VI)} = - \begin{pmatrix} X_1 s_1^2 c_2^2 + X_2 e^{2i\phi_1} + X_3 e^{2i\phi_2} & \frac{1}{2} X_1 s_1^2 \sin 2\theta_2 & \frac{1}{2} X_1 \sin 2\theta_1 c_2 \\ \frac{1}{2} X_1 s_1^2 \sin 2\theta_2 & X_1 s_1^2 s_2^2 & \frac{1}{2} X_1 \sin 2\theta_1 s_2 \\ \frac{1}{2} X_1 \sin 2\theta_1 c_2 & \frac{1}{2} X_1 \sin 2\theta_1 s_2 & X_1 c_1^2 \end{pmatrix} \quad (128)$$

$$\Delta^{(VI)} = 0 \quad (129)$$

(VII) There are one row and column components in which two elements are zero, and the common element on the both of such row and column is not zero.

$$\mathcal{U}^{(VII)} = \begin{pmatrix} 1 & 0 & 0 \\ 0 & c_1 & c_2 e^{i\phi_1} \\ 0 & s_1 & s_2 e^{i\phi_1} \end{pmatrix} \quad (130)$$

The effective mass matrix is

$$m_{eff}^{(VII)} = - \begin{pmatrix} X_1 & 0 & 0 \\ 0 & X_1 c_1^2 + X_3 c_2^2 e^{2i\phi_1} & \frac{1}{2} X_2 \sin 2\theta_1 + X_3 \sin 2\theta_2 e^{i(\phi_1+\phi_2)} \\ 0 & \frac{1}{2} (X_2 \sin 2\theta_1 + X_3 \sin 2\theta_2 e^{i(\phi_1+\phi_2)}) & X_1 s_1^2 + X_3 s_2^2 e^{2i\phi_2} \end{pmatrix} \quad (131)$$

$$\Delta^{(VII)} = 0 \quad (132)$$

Acknowledgement I would like to express my sincere gratitude to my supervisor, Dr.Takuya Morozumi for his elaborated guidance and discussions which are indispensable for my research. I would like to thank Dr.Yusuke Shimizu and Dr.Hiroyuki Umeeda for their valuable cooperation in my work. I also acknowledge the work of members in my laboratory for helpful discussions and comments.

References

- [1] Y. Fukuda *et al.* [Super-Kamiokande Collaboration], Phys. Rev. Lett. **81**, 1562 (1998) [hep-ex/9807003].
- [2] D. G. Michael *et al.* [MINOS Collaboration], Phys. Rev. Lett. **97**, 191801 (2006) [hep-ex/0607088].
- [3] K. Eguchi *et al.* [KamLAND Collaboration], Phys. Rev. Lett. **90**, 021802 (2003) [hep-ex/0212021].
- [4] Q. R. Ahmad *et al.* [SNO Collaboration], Phys. Rev. Lett. **89**, 011301 (2002) [nucl-ex/0204008]; Q. R. Ahmad *et al.* [SNO Collaboration], Phys. Rev. Lett. **89**, 011302 (2002) [nucl-ex/0204009].
- [5] F. P. An *et al.* [Daya Bay Collaboration], Phys. Rev. Lett. **108**, 171803 (2012) [arXiv:1203.1669 [hep-ex]].
- [6] J. K. Ahn *et al.* [RENO Collaboration], Phys. Rev. Lett. **108**, 191802 (2012) [arXiv:1204.0626 [hep-ex]].
- [7] Y. Abe *et al.* [Double Chooz Collaboration], Phys. Rev. D **86**, 052008 (2012) [arXiv:1207.6632 [hep-ex]].
- [8] K. Abe *et al.* [T2K Collaboration], Phys. Rev. Lett. **121**, no. 17, 171802 (2018) [arXiv:1807.07891 [hep-ex]].
- [9] M. A. Acero *et al.* [NOvA Collaboration], Phys. Rev. D **98**, 032012 (2018) [arXiv:1806.00096 [hep-ex]].
- [10] A. Gando *et al.* [KamLAND-Zen Collaboration], Phys. Rev. Lett. **117**, no. 8, 082503 (2016) Addendum: [Phys. Rev. Lett. **117**, no. 10, 109903 (2016)] [arXiv:1605.02889 [hep-ex]].
- [11] M. Agostini *et al.* [GERDA Collaboration], Phys. Rev. Lett. **120**, no. 13, 132503 (2018) [arXiv:1803.11100 [nucl-ex]].
- [12] P. Minkowski, Phys. Lett. **67B**, 421 (1977); T. Yanagida, in Proceedings of the Workshop on Unified Theories and Baryon Number in the Universe, eds. O. Sawada and A. Sugamoto (KEK report 79-18, 1979); M. Gell-Mann, P. Ramond and R. Slansky, Conf. Proc. C **790927**, 315 (1979) [arXiv:1306.4669 [hep-th]]; R. N. Mohapatra and G. Senjanovic, Phys. Rev. Lett. **44**, 912 (1980); J. Schechter and J. W. F. Valle, Phys. Rev. D **22**, 2227 (1980).
- [13] B. Adhikary, A. Ghosal and P. Roy, JHEP **0910**, 040 (2009)
- [14] B. Adhikary, M. Chakraborty and A. Ghosal, Phys. Rev. D **86**, 013015 (2012)
- [15] K. Asai, K. Hamaguchi, N. Nagata, S. Y. Tseng and K. Tsumura, Phys. Rev. D **99**, no. 5, 055029 (2019)
- [16] S. Choubey, W. Rodejohann and P. Roy, Nucl. Phys. B **808**, 272 (2009) Erratum: [Nucl. Phys. B **818**, 136 (2009)] [arXiv:0807.4289 [hep-ph]].

- [17] G. C. Branco, D. Emmanuel-Costa, M. N. Rebelo and P. Roy, *Phys. Rev. D* **77**, 053011 (2008)
- [18] B. Pontecorvo, *Sov. Phys. JETP* **7**, 172 (1958) [*Zh. Eksp. Teor. Fiz.* **34**, 247 (1957)].
- [19] Z. Maki, M. Nakagawa and S. Sakata, *Prog. Theor. Phys.* **28**, 870 (1962).
- [20] M. Kobayashi and T. Maskawa, *Prog. Theor. Phys.* **49**, 652 (1973). doi:10.1143/PTP.49.652
- [21] M. Doi, T. Kotani, H. Nishiura, K. Okuda and E. Takasugi, *Phys. Lett.* **102B**, 323 (1981).
- [22] T. Fujihara, S. Kaneko, S. K. Kang, D. Kimura, T. Morozumi and M. Tanimoto, *Phys. Rev. D* **72**, 016006 (2005)
- [23] C. Jarlskog, *Phys. Rev. Lett.* **55**, 1039 (1985).
- [24] T. Morozumi, in *Proceedings GUSTAVOFEST, CP Violation and the Flavour Puzzle*, p.113-118 (2005) [hep-ph/0512373].
- [25] M. C. Gonzalez-Garcia, M. Maltoni and T. Schwetz, *JHEP* **1411**, 052 (2014) [arXiv:1409.5439 [hep-ph]]; NuFIT 4.0 (2018), www.nu-fit.org/; I. Esteban, M. C. Gonzalez-Garcia, M. Maltoni, I. Martinez-Soler and T. Schwetz, *JHEP* **1701**, 087 (2017) [arXiv:1611.01514 [hep-ph]].